

Online estimation of biophysical neural networks

Thiago B. Burghi and Rodolphe Sepulchre

Abstract—This paper presents an adaptive observer for online state and parameter estimation of a broad class of biophysical models of neuronal networks. The design closely resembles classical solutions of adaptive control, and the convergence proof is based on contraction analysis. Our results include robustness guarantees with respect to unknown parameter dynamics. We discuss the potential of the approach in neurophysiological applications.

Index Terms—Adaptive control, Adaptive estimation, Nonlinear circuits, Nonlinear systems, Observers, Neuroscience.

I. INTRODUCTION

With the advancement of new technologies for measuring brain signals [23], [51], [54] it will be possible in the not-too-distant future to reliably and routinely record electrophysiological signals from large biological neural networks at cellular resolution. Such fine-grain data will open up new possibilities for the design of neural engineering systems such as brain-machine interfaces [41] and deep brain stimulation devices [35].

Any system designed to interface with the brain should take into account the adaptive nature of biological neural networks [50]. However, there are currently no established adaptive estimation or control paradigms for exploiting high-dimensional single-neuron intracellular recordings. A key difficulty arises from the spiking nature of electrophysiological signals, and the consequent nonlinearity of state-space models of biophysical neuronal systems [26], [29]. In particular, *conductance-based models*, introduced in the seminal work [21], have a large number of uncertain parameters and unmeasured states, and dealing with these issues has been an important modelling challenge [20], [30].

The question of estimating conductance-based neuronal models from input-output (i.e., current-voltage) data has mostly been approached with *offline* algorithms and *output-error* [2], [32] model structures. In the absence of noise in membrane voltage measurements, the prediction-error method [31] can be applied to estimate the model's inverse dynamics (mapping voltages to input currents), providing consistent estimates of the key parameters that shape neural behavior [8], [24]. Alternative methods estimate the forward dynamics instead, see e.g. [40], [42]. However, the forward dynamics

lack the fading memory property that is essential for dealing with output-error estimation criteria [31], [32], [36]. The spiking nature of neuronal models may thus lead to intractable optimization problems with nonsmooth cost functions and many spurious local minima [1], [45].

In this paper, we address the problem of *online* estimation of the key parameters in a conductance-based neuronal network: maximal conductances and reversal potentials. The former are implicated in the neuromodulation of neuronal behaviours, from the single-cell to the network scale [11], [13], [38], making them the natural biophysical targets for adaptive control. Our first contribution is to formulate this problem in terms of the online estimation of a class of *output feedback–contracting* nonlinear systems, that is, nonlinear systems whose dynamics can be made exponentially contracting [33] by output feedback. Output feedback contraction results from two system properties that are relevant to adaptive control: a (vector) relative degree one between input and output signals, and uniformly contracting internal dynamics [25]. Those structural properties of conductance-based were previously exploited in the batch method studied in our recent work [8].

Our second and main contribution consists in the design and convergence analysis of an *adaptive observer* for the general class of output feedback–contracting systems mentioned above. The proposed design is closely aligned with the literature on adaptive observers [3], [16], [17], [58], and the convergence proof is based on contraction theory [33]. Contraction analysis provides a proof of convergence reminiscent of the linear theory of adaptive control, as well as explicit convergence rates and robustness guarantees grounded in the concept of a *virtual system* [5], [55]. Contraction analysis has been a driving methodology in recent adaptive control research [34], [52], and the present work demonstrates its value for the design of adaptive systems in neuroscience.

The paper is organized as follows. The basic modelling assumptions of biophysical conductance-based models and their interconnection rules are reviewed in Section II. Section III highlights key system properties of conductance-based models, and motivates the problem of parameter estimation in these models. Section IV presents a general adaptive observer for conductance-based models, and includes the main convergence and robustness results. In Section V, we illustrate the performance of the adaptive observer and discuss the potential of the approach in neurophysiology.

A. Preliminaries

For a finite-dimensional vector x , we write $n_x := \dim(x)$. For two column vectors x and y , we write $\text{col}(x, y) :=$

Submitted to IEEE Transactions on Automatic Control. The research leading to these results has received funding from the European Research Council under the Advanced ERC Grant Agreement Switchlet n.670645.

Thiago B. Burghi and Rodolphe Sepulchre are with the Department of Engineering, Control Group, University of Cambridge, CB2 1PZ, UK (e-mails: tbb29@cam.ac.uk, r.sepulchre@eng.cam.ac.uk)

$(x^T, y^T)^T$. For a matrix $A \in \mathbb{R}^{n \times m}$, $\|A\|$ denotes the spectral norm (the largest singular value of A). For a vector $x \in \mathbb{R}^{n_x}$ and a symmetric matrix $P \in \mathbb{R}^{n_x \times n_x}$, we write $\|x\|_P^2 := x^T P x$, and $\|x\| := \|x\|_I$ with I the identity matrix. For a vector-valued function $f : \mathbb{R}^{n_1} \times \mathbb{R}^{n_2} \rightarrow \mathbb{R}^m$, we write $\partial_x f(x, y) \in \mathbb{R}^{m \times n_1}$ for the Jacobian of $f(x, y)$ with respect to x . Whenever there is no ambiguity, we omit the arguments of the Jacobian and write $\partial_x f = \partial_x f(x, y)$. We write $A \succeq B$ ($A \succ B$) if $A - B$ is a positive-semidefinite (positive-definite) matrix.

The system dynamics

$$\dot{x} = f(x, u) \quad (1)$$

is said to be *exponentially contracting* [33] in x on $X \subset \mathbb{R}^{n_x}$, uniformly in u on $U \subseteq \mathbb{R}^{n_u}$, if there exist a continuously differentiable symmetric matrix $P(x, t)$, called the *contraction metric*, and a constant $\lambda > 0$, called the *contraction rate*, such that $\epsilon_1 I \preceq P(x, t) \preceq \epsilon_2 I$ for some $\epsilon_1, \epsilon_2 > 0$, and $\partial_x f^T P + P \partial_x f + \dot{P} \preceq -2\lambda P$ for all $t \geq 0$, all $x \in X$, and all $u \in U$.

The set $X \subset \mathbb{R}^{n_x}$ is said to be *positively invariant* with respect to the dynamics (1), uniformly in u on $U \subseteq \mathbb{R}^{n_u}$, if $x(0) \in X$ and $u(t) \in U$ for all $t \geq 0$ imply $x(t) \in X$ for all $t \geq 0$. It is a well-known fact that if the dynamics (1) are exponentially contracting on a convex positively invariant set X , then all solutions of that system starting in X converge towards each other exponentially fast, with rate λ (for a proof of this statement, see for instance [28, Lemma 1]).

II. CONDUCTANCE-BASED MODELS

Starting with the seminal work of Hodgkin and Huxley [21], the nonlinear electrical circuits known as conductance-based models have become the foundation of biophysical modelling in neurophysiology. A detailed introduction to those models is found for instance in [26], [29]. This section shows that any conductance-based neural network model can be written in the form

$$\dot{v} = \Phi(v, w, u)\theta + b(v, w, u) \quad (2a)$$

$$\dot{w} = g(v, w) \quad (2b)$$

$$\dot{\theta} = 0 \quad (2c)$$

where $v(t) \in \mathbb{R}^{n_v}$ is a vector of measured output membrane voltages, $u(t) \in \mathbb{R}^{n_u}$ is a vector of input currents, $w(t) \in \mathbb{R}^{n_w}$ is a vector of unmeasured internal states, and $\theta \in \mathbb{R}^{n_\theta}$ is a vector of key biophysical parameters which we are interested in estimating. Because we shall perform parameter estimation using an adaptive observer, we regard θ as part of the state of the system, with the constant model (2c).

A. Conductance-based model of a single-neuron

In conductance-based modelling, every neuron is modelled as a one-port electrical circuit possessing the architecture shown in Figure 1: a capacitor of capacitance $c > 0$ in parallel with a *leak current* I_L and a number of *intrinsic ionic currents* I_{ion} . Additional extrinsic currents model the *synaptic currents* $I_{\text{syn},p}$, due to interconnections with other neurons, as well

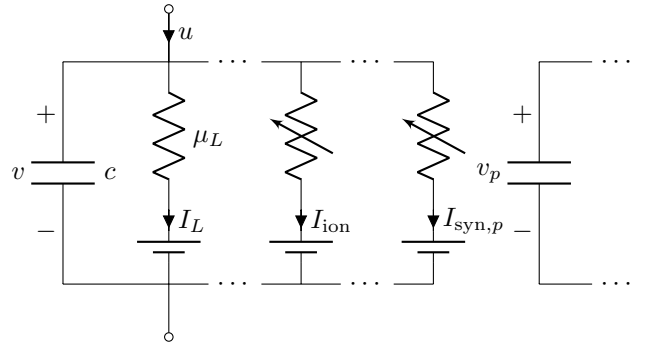


Fig. 1. Circuit representation of a neuron with voltage v that is coupled through a synapse to a presynaptic neuron with voltage v_p .

as an *input* (or *applied*) current u . The latter represents the current injected into the circuit by means of an intracellular electrode. The capacitor voltage v , which models the neuronal membrane potential, evolves according to Kirchhoff's law, that is

$$c \dot{v} = -I_L - \sum_{\text{ion} \in \mathcal{I}} I_{\text{ion}} - \sum_{\text{syn} \in \mathcal{S}} \sum_{p \in \mathcal{P}} I_{\text{syn},p} + u \quad (3)$$

where \mathcal{I} is the index set of intrinsic ionic currents, \mathcal{S} is the index set of synaptic neurotransmitter types, and \mathcal{P} is the index set of *presynaptic neurons*¹.

Each current in the circuit is Ohmic in nature, but with a conductance that can be nonlinear and voltage-dependent. The leak current has a constant conductance and is given by

$$I_L = -\mu_L(v - \nu_L),$$

whereas the intrinsic ionic currents are modelled by

$$I_{\text{ion}} = \mu_{\text{ion}} m_{\text{ion}}^{p_{\text{ion}}} h_{\text{ion}}^{q_{\text{ion}}} (v - \nu_{\text{ion}}) \quad (4a)$$

$$\tau_{m,\text{ion}}(v) \dot{m}_{\text{ion}} = -m_{\text{ion}} + \sigma_{m,\text{ion}}(v) \quad (4b)$$

$$\tau_{h,\text{ion}}(v) \dot{h}_{\text{ion}} = -h_{\text{ion}} + \sigma_{h,\text{ion}}(v) \quad (4c)$$

The constants $\mu_{\text{ion}} > 0$ and $\nu_{\text{ion}} \in \mathbb{R}$ are called (intrinsic) *maximal conductances* and *reversal potentials*, respectively. The static *activation functions* $\sigma_{m,\text{ion}}(v)$ and $\sigma_{h,\text{ion}}(v)$, and *time-constant functions* $\tau_{m,\text{ion}}(v)$ and $\tau_{h,\text{ion}}(v)$, model the nonlinear gating of the ionic conductance. The activation functions are given by sigmoid functions of the form²

$$\sigma(v) = \frac{1}{1 + \exp(-(v - \rho)/\kappa)}, \quad (5)$$

The constants $\rho_{m,\text{ion}} \in \mathbb{R}$ and $\rho_{h,\text{ion}} \in \mathbb{R}$ determine the inflection points of the activation functions, while the constants $\kappa_{m,\text{ion}} > 0$ and $\kappa_{h,\text{ion}} < 0$ determine their slopes. Because $\sigma_{m,\text{ion}} : \mathbb{R} \rightarrow (0, 1)$ and $\sigma_{h,\text{ion}} : \mathbb{R} \rightarrow (0, 1)$ are monotonically increasing and decreasing, respectively, the states m_{ion} and h_{ion} are called *activation* and *inactivation gating variables*, respectively. The time-constant functions vary in shape, but always respect the bounds

$$0 < \tau_{\text{ion}} \leq \tau_{m,\text{ion}}(v), \tau_{h,\text{ion}}(v) \leq \bar{\tau}_{\text{ion}}$$

¹A trivial extension of this formulation allows for considering multicompartment models and gap junction currents (linear diffusive coupling).

²Some models are defined with a different type of sigmoid. The results in this paper hold for any continuous function with range on $(0, 1)$.

for all $v \in \mathbb{R}$ and some $\tau_{\text{ion}}, \bar{\tau}_{\text{ion}} > 0$. The exponents p_{ion} and q_{ion} in (4a) are natural numbers (including zero).

Example 1. The Hodgkin-Huxley (HH) model, introduced in the seminal paper [21], includes two intrinsic ionic currents: a transient sodium current I_{Na} and a potassium current I_{K} , so that $\mathcal{I} = \{\text{Na}, \text{K}\}$. The voltage dynamics of a single, isolated HH model (no synaptic currents) are given by

$$c\dot{v} = - \underbrace{\mu_{\text{Na}} m_{\text{Na}}^3 h_{\text{Na}} (v - \nu_{\text{Na}})}_{I_{\text{Na}}} - \underbrace{\mu_{\text{K}} m_{\text{K}}^4 (v - \nu_{\text{K}})}_{I_{\text{K}}} - \underbrace{\mu_{\text{L}} (v - \nu_{\text{L}})}_{I_{\text{L}}} + u$$

and the gating variable dynamics are of the form (4b)-(4c) for $\text{ion} \in \{\text{Na}, \text{K}\}$. We will return to the HH model in Sections III and V.

Synaptic currents arise from electrochemical connections between neurons [15, Chapter 7]. We consider the model used in [10], [15], which can be written as

$$I_{\text{syn},p} = \mu_{\text{syn},p} s_{\text{syn},p} (v - \nu_{\text{syn}}) \quad (6a)$$

$$\tau_{\text{syn}}(v_p) \dot{s}_{\text{syn},p} = -s_{\text{syn},p} + a_{\text{syn}} \tau_{\text{syn}}(v_p) \sigma_{\text{syn}}(v_p) \quad (6b)$$

with a synaptic time-constant function τ_{syn} given by

$$\tau_{\text{syn}}(v_p) = \frac{1}{a_{\text{syn}} \sigma_{\text{syn}}(v_p) + b_{\text{syn}}} \quad (7)$$

and a synaptic activation function σ_{syn} of the form (5), with $\rho_{\text{syn}} \in \mathbb{R}$ and $\kappa_{\text{syn}} > 0$. Here, $s_{\text{syn},p}$ is the synaptic gating variable, v_p is the membrane voltage of the presynaptic neuron, and $a_{\text{syn}} > 0$ and $b_{\text{syn}} > 0$ are constant parameters. The constants $\mu_{\text{syn},p} > 0$ and $\nu_{\text{syn}} \in \mathbb{R}$ are (synaptic) maximal conductances and reversal potentials, respectively, and the synaptic time-constant function respects the bounds

$$0 < \tau_{\text{syn}} \leq \tau_{\text{syn}}(v_p) \leq \bar{\tau}_{\text{syn}}$$

for all $v_p \in \mathbb{R}$, with $\tau_{\text{syn}} = 1/(a_{\text{syn}} + b_{\text{syn}})$ and $\bar{\tau}_{\text{syn}} = 1/b_{\text{syn}}$. This model can represent excitatory or inhibitory synapses, depending on the value of ν_{syn} .

B. Conductance-based model of a neural network

A conductance-based neural network is given by the interconnection of $n_v \in \mathbb{N}$ single neurons via synaptic currents. We denote the index set of neurons in the network by

$$\mathcal{N} := \{1, \dots, n_v\}$$

and we describe the dynamics of the i^{th} neuron in the network by attaching an $i \in \mathcal{N}$ subscript to all the variables in (3)-(6), except for reversal potentials, time-constant functions, and activation functions. The network's state-space model can be found by collecting all neuronal membrane voltages in the vector

$$v = (v_1, \dots, v_{n_v})^{\text{T}},$$

and all gating variables in the vector

$$w = \text{col}(w^{(1)}, \dots, w^{(n_v)}),$$

where the vector $w^{(i)}$ collects the intrinsic and synaptic gating variables of the i^{th} neuron, that is, $m_{\text{ion},i}$, $h_{\text{ion},i}$, and $s_{\text{syn},p,i}$. Notice that with this notation, $\mathcal{P} \subseteq \mathcal{N}$.

Example 2. A Half-Center Oscillator (HCO) is a network composed of two neurons mutually coupled by inhibitory synapses. This elementary network is the simplest example of a Central Pattern Generator, a type of neural network that plays an important role in the generation of autonomous rhythms for motor control [37]. As detailed in [10], a simple HCO model is obtained by interconnecting two HH neurons with a GABA-type synaptic current I_{G} , and adding to each of the neurons an intrinsic calcium current I_{Ca} . This results in $\mathcal{I} = \{\text{Na}, \text{K}, \text{Ca}\}$, $\mathcal{S} = \{\text{G}\}$, and voltage dynamics given by

$$\begin{aligned} c_i \dot{v}_i = & -\mu_{\text{Na},i} m_{\text{Na},i}^3 h_{\text{Na},i} (v_i - \nu_{\text{Na}}) - \mu_{\text{K},i} m_{\text{K},i}^4 (v_i - \nu_{\text{K}}) \\ & - \mu_{\text{Ca},i} m_{\text{Ca},i}^3 h_{\text{Ca},i} (v_i - \nu_{\text{Ca}}) - \mu_{\text{G},p,i} s_{\text{G},p,i} (v_i - \nu_{\text{G}}) \\ & - \mu_{\text{L},i} (v_i - \nu_{\text{L}}) + u_i \end{aligned}$$

for $i, p \in \mathcal{N} = \{1, 2\}$ and $p \neq i$. The gating variables of each neuron, which evolve according to (4b)-(4b) and (6b), are collected in $w^{(i)} = (m_{\text{Na},i}, h_{\text{Na},i}, m_{\text{K},i}, m_{\text{Ca},i}, h_{\text{Ca},i}, s_{\text{G},i,p})^{\text{T}}$.

Any conductance-based network whose neurons have the dynamics (3)-(6) can be written in the form (2), which emphasizes the affine dependence of the network voltage dynamics on a constant parameter vector $\theta \in \mathbb{R}^{n_\theta}$. The vector function $g(v, w)$ in (2b) can be found by collecting the dynamics of all gating variables in the network, respecting the order in which those variables were included in w . For each neuron in the network, these dynamics are easily found from (4b), (4c), and (6b).

For a given conductance-based network, there are multiple ways to obtain a parametrization of the form (2a). This is because there are multiple ways to define θ based on the biophysical parameters of the voltage dynamics — capacitances, maximal conductances and reversal potentials. The choice of a particular parametrization is dictated by the biophysical parameters to be estimated, and determines the contents of the matrix $\Phi(v, w, u)$ and the vector $b(v, w, u)$. The following example illustrates a convenient parametrization that can be used when all capacitances, maximal conductances and reversal potentials must be estimated:

Example 3. (Lumped parametrization) Consider the HH model in Example 1. We can *lump* the biophysical parameters of the voltage dynamics in the vector θ according to

$$\theta = \frac{1}{c} (\mu_{\text{Na}}, \mu_{\text{K}}, \mu_{\text{L}}, \mu_{\text{Na}} \nu_{\text{Na}}, \mu_{\text{K}} \nu_{\text{K}}, \mu_{\text{L}} \nu_{\text{L}}, 1)^{\text{T}}$$

Letting $w = (m_{\text{Na}}, h_{\text{Na}}, m_{\text{K}})^{\text{T}}$, the voltage dynamics of the model can then be written as (2a), where

$$\Phi(v, w, u) = \begin{pmatrix} -m_{\text{Na}}^3 h_{\text{Na}} v \\ -m_{\text{K}}^4 v \\ -v \\ m_{\text{Na}}^3 h_{\text{Na}} \\ m_{\text{K}}^4 \\ 1 \\ u \end{pmatrix}^{\text{T}} \quad (8)$$

and $b = 0$. The vector field $g(v, w)$ can be found from (4b)-(4c) for $\text{ion} \in \{\text{Na}, \text{K}\}$. Notice that, for a given value of θ , we can uniquely recover the values of the biophysical parameters above. For instance, we have $c = \theta_7^{-1}$, $\mu_{\text{Na}} = \theta_1 \theta_7^{-1}$, and $\nu_{\text{Na}} = \theta_1^{-1} \theta_4$. This example can be easily generalized to the case of a network with $n_v > 1$ neurons.

Estimation of the *maximal conductance* parameters is of particular importance in neurophysiological applications, as they can be regarded as the key parameters for *adaptive* control of a neuronal network [11]–[13]. Maximal conductances model the level of expression of particular types of ion channels in the neuron [20], and a key objective of neurophysiology is to understand how neuromodulators affect these parameters [38]. In contrast, the other biophysical parameters of a neuron may often be assumed to be known and constant. The following example illustrates a parametrization based exclusively on maximal conductances:

Example 4. Consider the HCO model in Example 2, and let

$$\mu^{(i)} = (\mu_{\text{Na},i}, \mu_{\text{K},i}, \mu_{\text{Ca},i}, \mu_{\text{G},p,i}, \mu_{\text{L},i})^\top \quad (9)$$

for $i, p \in \mathcal{N} = \{1, 2\}$ and $p \neq i$. Then we can parameterize the HCO according to

$$\theta = \text{col}(\mu^{(1)}, \mu^{(2)}) \quad (10)$$

with $\mu^{(1)}$ and $\mu^{(2)}$ given by (9). Letting $v = (v_1, v_2)^\top$ and $w = \text{col}(w^{(1)}, w^{(2)})$, the voltage dynamics of the model can then be written as (2a), where

$$\Phi(v, w) = \begin{bmatrix} \varphi(v_1, w^{(1)}) & 0 \\ 0 & \varphi(v_2, w^{(2)}) \end{bmatrix}$$

$$b(t) = (u_1(t)/c_1, u_2(t)/c_2)^\top$$

with

$$\varphi(v_i, w^{(i)}) = -\frac{1}{c_i} \begin{pmatrix} m_{\text{Na},i}^3 h_{\text{Na},i} (v_i - \nu_{\text{Na}}) \\ m_{\text{K},i}^4 (v_i - \nu_{\text{K}}) \\ m_{\text{Ca},i}^3 h_{\text{Ca},i} (v_i - \nu_{\text{Ca}}) \\ s_{\text{G},p,i} (v_i - \nu_{\text{G}}) \\ v_i - \nu_{\text{L}} \end{pmatrix}^\top$$

for $i = 1, 2$ and $p \neq i$.

A significant property of the parametrization in Example 4 is that it is decentralised: the network estimation problem decouples into independent single-neuron estimation problems. This decoupling makes the estimation problem scalable to a high-dimensional network.

III. SYSTEM PROPERTIES OF CONDUCTANCE-BASED MODELS

The neuronal behaviours displayed by the conductance-based model (2) range from the simple spiking oscillations of single neurons to the large-scale rhythmic computations performed by cortical networks [56]. Despite their complexity, conductance-based networks have fundamental properties which are central to observer design and parameter estimation. In this section, we first discuss these properties. Then, as a

motivation for our main results in Section IV, we discuss the difficulties associated with batch-mode parameter estimation in these models, and propose a simple solution to the problem.

A. System properties

1) *Positively invariant sets:* For uniformly bounded inputs, the nonlinear behaviours of conductance-based models can be shown to lie within a bounded region of the state-space. This is because maximal conductances are always positive, a constraint that allows the construction of a positively invariant set for (2):

Proposition 1. *Let (2) describe a conductance-based network, and let $U \subset \mathbb{R}^{n_v}$ be a compact set. Then the set*

$$[v_{\min}, v_{\max}]^{n_v} \times [0, 1]^{n_w} \quad (11)$$

is positively invariant with respect to (2a)-(2b), uniformly on U , where

$$v_{\max} := \max \left\{ \max_{\text{ion}} \nu_{\text{ion}}, \max_{\text{syn}} \nu_{\text{syn}}, \frac{\bar{u}}{\underline{\mu}_{\text{L}}} + \nu_{\text{L}} \right\}$$

$$v_{\min} := \min \left\{ \min_{\text{ion}} \nu_{\text{ion}}, \min_{\text{syn}} \nu_{\text{syn}}, -\frac{\bar{u}}{\underline{\mu}_{\text{L}}} + \nu_{\text{L}} \right\}$$

with $\bar{u} := \sup_{u \in U} \|u\|_\infty$ and $\underline{\mu}_{\text{L}} = \min_{i \in \mathcal{N}} \mu_{\text{L},i}$.

Proof. We begin by noticing that $[0, 1]^{n_w}$ is a positively invariant set for (2b), uniformly in v on \mathbb{R}^{n_v} . This follows by inspection of (4b)-(4c) and (6b), which reveals that none of the gating variables in the network are able to leave the interval $[0, 1]$. For instance, $\dot{m}_{\text{ion},i} \geq 0$ for $m_{\text{ion},i} = 0$ and all $v_i \in \mathbb{R}$, and $\dot{m}_{\text{ion},i} \leq 0$ for $m_{\text{ion},i} = 1$ and all $v_i \in \mathbb{R}$ ($i \in \mathcal{N}$). Now, assuming $w(0) \in [0, 1]^{n_w}$, since all gating variables remain nonnegative for all $t \geq 0$, we are able to show that each v_i cannot leave the interval $[v_{\min}, v_{\max}]$, proving the result. This follows by inspection of (3) for each neuron in the network: if $v_i = v_{\max}$, then $\dot{v}_i \leq 0$, whereas if $v_i = v_{\min}$, then $\dot{v}_i \geq 0$. \square

2) *Exponentially contracting internal dynamics:* A conductance-based network model given by the nonlinear system (2) has a global vector relative degree [25] equal to one: Kirchoff's equation implies

$$\partial_u \dot{v} = \text{diag}(1/c_i)$$

Moreover, its internal dynamics (2b), with input v and state vector w , are exponentially contracting:

Proposition 2. *The internal dynamics (2b) of a conductance-based network model are exponentially contracting on the positively invariant set $[0, 1]^{n_w}$, uniformly in v on \mathbb{R}^{n_v} . Exponential contraction holds with a diagonal constant contraction metric and a contraction rate given by $\bar{\tau}^{-1}$, where*

$$\bar{\tau} = \max \left\{ \max_{\text{ion}} \bar{\tau}_{\text{ion}}, \max_{\text{syn}} \bar{\tau}_{\text{syn}} \right\} \quad (13)$$

is an upper bound for all gating variable time-constant functions.

Proof. The uniform positive invariance of $[0, 1]^{n_w}$ was shown in the proof of Proposition 1. To verify uniform contraction, it suffices to show that, for any neuron in the network, the dynamics of each of its gating variables are exponentially contracting on $[0, 1]$, uniformly in v , with a contraction rate given by the inverse of $\bar{\tau}_{\text{ion}}$ (for intrinsic gating variables) or $\bar{\tau}_{\text{syn}}$ (for synaptic ones). The result then follows from the fact that (2b) is a parallel interconnection of exponentially contracting systems, uniformly in v [49]. For completion, we show contraction of the dynamics of an arbitrary m_{ion} , with the proof for other gating variables being identical. The differential dynamics of m_{ion} are given by

$$\delta \dot{m}_{\text{ion}} = -\tau_{m_{\text{ion}}}(v)^{-1} \delta m_{\text{ion}}$$

where $-\tau_{m_{\text{ion}}}(v)^{-1} = \partial \dot{m}_{\text{ion}} / \partial m_{\text{ion}}$ is a one-dimensional Jacobian. This Jacobian satisfies

$$-\tau_{m_{\text{ion}}}(v)^{-1} P_{m_{\text{ion}}} - P_{m_{\text{ion}}} \tau_{m_{\text{ion}}}(v)^{-1} \leq -2 \bar{\tau}_{\text{ion}}^{-1} P_{m_{\text{ion}}}$$

for any $P_{m_{\text{ion}}} > 0$. Thus the dynamics of m_{ion} are exponentially contracting on $[0, 1]$, uniformly in v , with contraction rate $\bar{\tau}_{\text{ion}}^{-1}$. \square

Remark 1. Proposition 2 implies that the system

$$\dot{\hat{w}} = g(v, \hat{w}) \quad (14)$$

is an exponentially convergent reduced-order identity observer for the dynamics (2a)-(2b). More precisely, $\hat{w}(t) \rightarrow w(t)$ as $t \rightarrow \infty$ for any piecewise continuous $v(t)$ and any initial conditions $\hat{w}(0), w(0) \in [0, 1]^{n_w}$ (cf. [33, Example 3.3] or [49, Example 2.5]).

3) Output feedback contraction: The two properties of Propositions 1 and 2 together imply that conductance-based models are *output feedback contracting*, in the sense that the simple (proportional) output feedback $u = -\gamma v$ makes the closed-loop feedback system exponentially contracting on the invariant set of Proposition 1 for sufficiently large $\gamma > 0$ (see [8, Proposition 2] for the single-neuron case). The role of output feedback is to compensate for intrinsic and extrinsic currents providing positive feedback to the membrane dynamics. Output feedback contraction has been explored for batch estimation of conductance-based models in [1] and [8].

B. Positive feedback and output-error estimation issues

Conductance-based models have contracting inverse dynamics, but possibly non-contracting forward dynamics. In the terminology of linear systems, they have stable zeros, but possibly unstable poles. This is because their intrinsic currents include negative conductance elements, a source of positive feedback and instability that is essential to excitability and spiking [46].

Example 5. Consider the HH model of Example 1, with reversal potentials such that $\nu_K < \nu_L < \nu_{\text{Na}}$. For any input current such that $|u(t)| < \mu_L(\nu_{\text{Na}} - \nu_L)$ for all $t \geq 0$, the bounds (12) in Proposition 1 show that the membrane voltage satisfies $v < \nu_{\text{Na}}$ for all $t \geq 0$. This implies that

$$-\partial_{m_{\text{Na}}} I_{\text{Na}} \partial_v \dot{m}_{\text{Na}} > 0$$

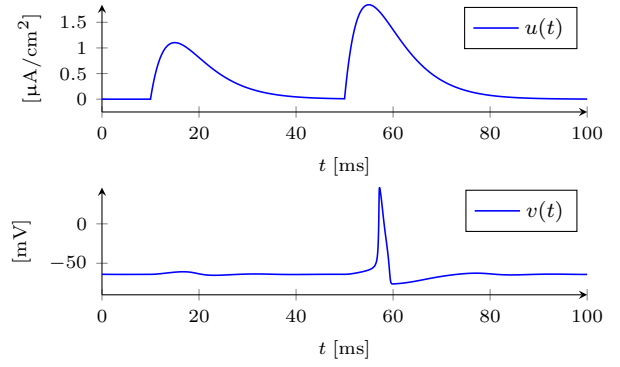


Fig. 2. Excitability in the HH model. A small current pulse causes no spike, while a larger current pulse causes a spike. The figure was obtained using HH parameter values described in Table I and Appendix C.1.

at any admissible equilibrium of the system, and thus the Sodium current I_{Na} introduces positive feedback to the membrane voltage of the HH model.

The non-contracting nature of the forward dynamics is the main reason why traditional parameter estimation methods based on *output-error* (or *simulation-error*) criteria [32], [36] cannot be straightforwardly applied to conductance-based models. This is illustrated by means of a numerical example:

Example 6. Consider the typical biophysical parameters of the HH model shown in Table I below. Owing to the large value of μ_{Na} , the positive feedback introduced by the Sodium current I_{Na} dominates the model dynamics in some regions of the state-space [26]. Using these parameters, Figure 2 illustrates the excitability of the model.

Now, consider the parametrization given by $\theta = \mu_{\text{Na}}$, and suppose μ_{Na} must be estimated from the continuous-time measurements $u(t)$ and $v(t)$ shown in Figure 2. In a naive application of the prediction-error method [32], we propose a *predictor model* given by

$$\begin{aligned} \dot{c}\hat{v} &= -\hat{\mu}_{\text{Na}} \hat{m}_{\text{Na}}^3 \hat{h}_{\text{Na}} (\hat{v} - \nu_{\text{Na}}) + b(\hat{v}, \hat{m}_{\text{K}}, u) \\ \dot{\hat{w}} &= g(\hat{v}, \hat{w}) \end{aligned} \quad (15)$$

with $\hat{w} = (\hat{m}_{\text{Na}}, \hat{h}_{\text{Na}}, \hat{m}_{\text{K}})^T$ and

$$b(\hat{v}, \hat{m}_{\text{K}}, u) = -\mu_{\text{K}} \hat{m}_{\text{K}}^4 (\hat{v} - \nu_{\text{K}}) - \mu_{\text{L}} (\hat{v} - \nu_{\text{L}}) + u$$

and then estimate $\hat{\mu}_{\text{Na}}$ by minimizing the *output-error* cost function

$$V(\hat{\mu}_{\text{Na}}, \hat{w}(0), T) = \frac{1}{T} \int_0^T (v(t) - \hat{v}(t))^2 dt \quad (16)$$

in $\hat{\mu}_{\text{Na}}$ and $\hat{w}(0)$. The issue with this approach is that it may not be trivial to find a global minimum for $\hat{\mu}_{\text{Na}}$ using numerical methods, even when the problem is simplified

TABLE I
PARAMETERS OF THE HH MODEL [22], [26].

μ_{Na}	μ_{K}	μ_{L}	ν_{Na}	ν_{K}	ν_{L}	c
120	36	0.3	55	-77	-54.4	1

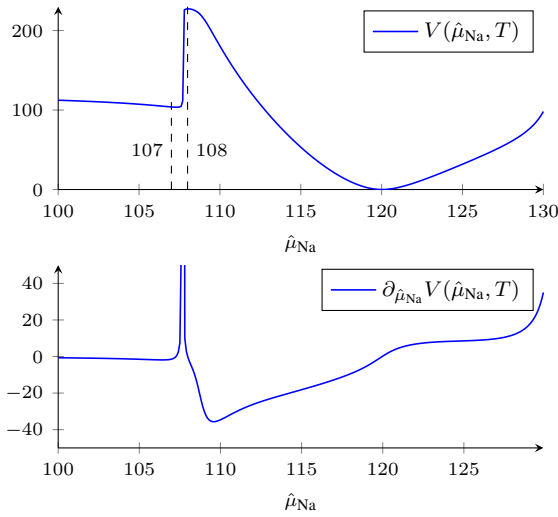


Fig. 3. Cost function $V(\hat{\mu}_{\text{Na}}, w(0), T)$ given by (16) and its gradient.

by fixing $(\hat{v}(0), \hat{w}(0)) = (v(0), w(0))$. The reason can be visualized in Figure 3, where we have plotted the cost function $V(\hat{\mu}_{\text{Na}}, w(0), T)$ obtained with the input-output traces from Figure 2 ($T = 100$). It can be seen that the cost function is nearly discontinuous between $\hat{\mu}_{\text{Na}} = 107$ and $\hat{\mu}_{\text{Na}} = 108$. The behaviour underlying this near discontinuity is unveiled in Figure 4, where two solutions of (15) are plotted corresponding to the estimates $\hat{\mu}_{\text{Na}} = 107$ and $\hat{\mu}_{\text{Na}} = 108$. It is the spike which appears when increasing $\hat{\mu}_{\text{Na}}$ that causes a sudden change in the cost function. The cost function contains one near discontinuity, since there is a single spike being fired. For a dataset with multiple spikes, the cost function would rapidly become intractable.

Example 6 illustrates the more general problem of lack of tractability in estimating the parameters of a non-contracting system with an output-error criterion [1], [45]. In fact, the lack of contraction is the root cause of what has been called the ‘‘exploding gradient’’ problem in deep learning theory [43]. The exploding gradient is clearly visible in Figure 3.

C. Voltage equation-error estimation

To remedy the instability illustrated in Example 6, we can make use of Remark 1 and employ the reduced-order observer (14) to obtain estimates \hat{w} of the internal states w . Contraction of the internal states suggests postulating the predictor model

$$\dot{\hat{v}} = \Phi(v, \hat{w}, u)\hat{\theta} + b(v, \hat{w}, u) \quad (17a)$$

$$\dot{\hat{w}} = g(v, \hat{w}) \quad (17b)$$

which, in the particular case of Example 6, amounts to replacing \hat{v} by v in the right-hand side of (15).

Notice that, for $\hat{w} = w$, the voltage predictor model (17a) acquires a continuous-time *equation-error* model structure [2], [32]. Classical system identification theory [2, Section 2] thus hints that parameter estimation can be performed by solving the problem

$$\hat{\theta}_T = \min_{\hat{\theta}} V(\hat{\theta}, T) \quad (18)$$

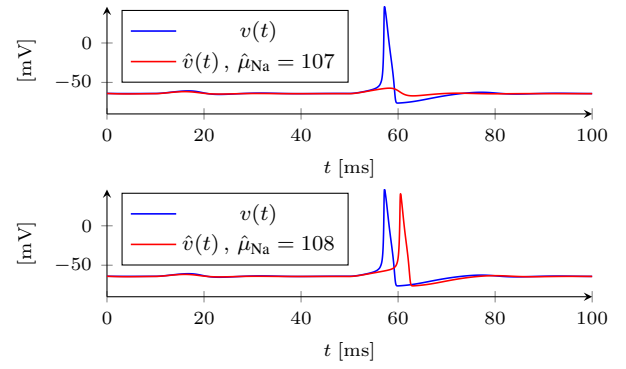


Fig. 4. Solutions of the HH predictor (15) for two values of $\hat{\mu}_{\text{Na}}$ (red), compared to the solution of the true model displayed in Figure 2 (blue).

with the weighted cost function

$$V(\hat{\theta}, T) = \frac{1}{T} \int_0^T e^{-\alpha(t-\tau)} \|H\dot{v}(\tau) - H\dot{\hat{v}}(\tau)\|^2 d\tau \quad (19)$$

where $\alpha > 0$ is a *forgetting factor*, introduced to discount the initial error between $w(0)$ and $\hat{w}(0)$, and H is the operator of a strictly proper LTI filter introduced to avoid differentiating $v(t)$. Choosing the simple filter

$$H(s) = \frac{\gamma}{s + \gamma} \quad (20)$$

leads to

$$\begin{aligned} H\dot{\hat{v}}(t) &= \gamma\Psi(t)\hat{\theta} + H\hat{b}(t) \\ \dot{\Psi}(t) &= -\gamma\Psi(t) + \Phi(v(t), \hat{w}(t), u(t)) \\ \hat{b}(t) &= b(v(t), \hat{w}(t), u(t)) \end{aligned} \quad (21)$$

which shows that (19) is now quadratic in $\hat{\theta}$ (notice $H\dot{v}$ can be obtained by filtering the data v with $sH(s)$). It follows that the batch-mode problem (18) admits a well-known solution based on the normal equation [2, p. 55]. The fact that $\hat{\theta}_T \rightarrow \theta$ as $T \rightarrow \infty$ will be shown to be a consequence of the convergence properties of the adaptive observer introduced in Section IV.

IV. AN ADAPTIVE OBSERVER FOR CONDUCTANCE-BASED MODELS

A. Contraction-based observer design

Consider any system of the form (2), where $v(t) \in \mathbb{R}^{n_v}$ is a measured output, $w(t) \in \mathbb{R}^{n_w}$ are unmeasured internal states, $\theta(t) \in \mathbb{R}^{n_\theta}$ are unknown parameters which we wish to estimate, and Φ , b and g are continuously differentiable functions of the appropriate dimensions. The parameters are considered as system states, with $\theta(t) = \theta(0)$ for all $t \geq 0$.

The proposed adaptive observer is given by

$$\begin{aligned} \dot{\hat{v}} &= \Phi(v, \hat{w}, u)\hat{\theta} + b(v, \hat{w}, u) + \gamma(I + \Psi P \Psi^\top)(v - \hat{v}) \\ \dot{\hat{w}} &= g(v, \hat{w}) \\ \dot{\hat{\theta}} &= \gamma P \Psi^\top (v - \hat{v}) \end{aligned} \quad (22)$$

where $\gamma > 0$ is a constant gain, and the matrices P and Ψ evolve according to

$$\dot{\Psi} = -\gamma\Psi + \Phi(v, \hat{w}, u), \quad \Psi(0) = 0 \quad (23a)$$

$$\dot{P} = \alpha P - P \Psi^\top \Psi P, \quad P(0) \succ 0 \quad (23b)$$

where $\alpha > 0$ is a constant forgetting rate. The assumption that $\Psi(0) = 0$ is made without loss of generality. Our main goal in this section is to study the convergence properties of the adaptive observer (22)-(23).

An intuitive understanding of the design (22)-(23) can be gained from the following:

Proposition 3. *The adaptive observer (22)-(23) recursively solves the weighted least squares problem given by (2) and (18)-(21).*

Proof. By [2, Theorem 2.5], the Recursive Least Squares (RLS) solution to (18)-(21) is given by

$$\dot{\hat{\theta}}(t) = P(t)\Psi(t)^\top(H\dot{v}(t) - \gamma\Psi(t)\hat{\theta}(t) - H\hat{b}(t)) \quad (24)$$

with P given by (23b). Thus (22)-(23) implements the RLS solution to (18)-(21) if and only if

$$H\dot{v}(t) - \gamma\Psi(t)\hat{\theta}(t) - H\hat{b}(t) = \gamma(v - \hat{v}) \quad (25)$$

To verify the above identity, we first notice that

$$\begin{aligned} \frac{d}{dt}(\Psi\hat{\theta}) &= -\gamma\Psi\hat{\theta} + \Phi\hat{\theta} + \gamma\Psi P\Psi^\top(v - \hat{v}) \\ &= -\gamma\Psi\hat{\theta} + \dot{v} - \gamma(v - \hat{v}) - \hat{b} \end{aligned}$$

Solving the previous equation for $\Psi\hat{\theta}$ and multiplying the result by γ , we obtain

$$\gamma\Psi(t)\hat{\theta}(t) = -\gamma H v(t) - H\hat{b}(t) + \gamma\hat{v}(t)$$

We can now recover (25) by adding $\gamma(v(t) - \hat{v}(t))$ to both sides of the previous equation and applying the identity

$$\gamma(v(t) - H v(t)) = H\dot{v}(t)$$

which can be easily verified from (20). \square

Remark 2. The adaptive observer (22)-(23) relates to a number of designs in the literature. For instance, when we set $P = I$, $\Psi = \Phi$, and remove both the the adaptive gain $\Psi P \Psi^\top$ in (22) and its dynamics (23), the adaptive observer above reduces to the simple design proposed in [3]. When we remove the internal dynamics ($n_w = 0$), then (22)-(23) is reminiscent of the high-gain design proposed in [16], who used it for uniformly observable systems with one-to-one (possibly nonlinear) parametrizations. The roots behind the design of [16] can be traced back to the early high-gain nonlinear observer of [17] and the linear adaptive observer of [58].

In what follows, we will show that the convergence of the adaptive observer above does not require a high gain. In fact, the distinction between the forgetting rate α and the gain γ will play a role both in our convergence proof and in a practical context where it is beneficial to tune these gains separately.

We now formalize the following two assumptions, which have been proved to hold for the particular case of conductance-based models in Section III:

Assumption 1. There exists a compact set $V \times U$ such that $\{v(t), u(t)\} \in V \times U$ for all $t \geq 0$.

Assumption 2. There exists a compact convex set W which is positively invariant with respect to (2b), uniformly in v on

\mathbb{R}^{n_v} . Furthermore, there exist a symmetric matrix $M_1(t)$ such that

$$\sigma_1 I \preceq M_1(t) \preceq \sigma_2 I \quad (26)$$

for some $\sigma_1, \sigma_2 > 0$, and a contraction rate $\lambda_1 > 0$ such that

$$Q_1 = \partial_w g(v, w)^\top M_1 + M_1 \partial_w g(v, w) + \dot{M}_1 \quad (27)$$

satisfies

$$Q_1 \preceq -2\lambda_1 M_1 \quad (28)$$

for all $\{v, w\} \in \mathbb{R}^{n_v} \times W$ and all $t \geq 0$.

In other words, the internal dynamics (2b) are exponentially contracting on the invariant set W , uniformly in v . Notice this also applies to the dynamics of \hat{w} in (22), which only differs from (2b) in the initial condition.

We will also require a standard persistent excitation condition (see, for instance, [3], [16], [53]):

Assumption 3. The signals $v(t)$ and $u(t)$ are such that for any trajectory of (22), there exist $T > 0$ and $\delta > 0$ such that for all $t \geq 0$,

$$\delta I \preceq \int_t^{t+T} \Psi^\top(\tau)\Psi(\tau)d\tau$$

Our main convergence result can now be stated:

Theorem 1. *Consider the systems (2) and (22)-(23), and let Assumptions 1 to 3 hold. Let $\alpha > 0$ and*

$$\gamma > \min\{\alpha, \lambda_1, 1\}.$$

Then, for any $\hat{v}(0) \in \mathbb{R}^{n_v}$, $\hat{w}(0) \in W$, and $\hat{\theta}(0) \in \mathbb{R}^{n_\theta}$, we have

$$\text{col}(\hat{v}(t), \hat{w}(t), \hat{\theta}(t)) \rightarrow \text{col}(v(t), w(t), \theta(t))$$

exponentially fast as $t \rightarrow \infty$, with a convergence rate given by $\min\{\alpha, \lambda_1\}$.

Proof. The proof relies on the *virtual system* idea from contraction analysis [33], [55]: we construct a system (the virtual system) whose solutions contain the solutions of both (2) and (22), and then show that such a system is exponentially contracting on a positively invariant set. This implies that all solutions of (2) and (22) exponentially contract to the same solution within that set. The virtual system we consider is given by

$$\dot{s} = g(v, s) \quad (29a)$$

$$\dot{r} = a(t, s, \eta) + b(v, s, u) + \gamma(I + \Psi P \Psi^\top)(v - r) \quad (29b)$$

$$\dot{\eta} = \beta P \Psi^\top(v - r) \quad (29c)$$

where

$$a(t, s, \eta) = \Phi(v, s, u)\theta + \Phi(v, \hat{w}, u)\eta - \Phi(v, \hat{w}, u)\theta$$

and s, r and η are the virtual system states³. Notice that since $a(t, w, \theta) = \Phi(v, w, u)\theta$ and $a(t, \hat{w}, \hat{\theta}) = \Phi(v, \hat{w}, u)\hat{\theta}$, any solutions $\text{col}(w, v, \theta)$ of (2) and $\text{col}(\hat{w}, \hat{v}, \hat{\theta})$ of (22) are particular solutions of the virtual system (29).

³We emphasize the time-dependence of a due to the signals $v(t)$, $\hat{w}(t)$, and $u(t)$, which are not states of the virtual system.

Assumption 2 implies that the convex set $W \times \mathbb{R}^{n_v} \times \mathbb{R}^{n_\theta}$ is positively invariant with respect to (29). Thus, all we need to show is that (29) is exponentially contracting on $W \times \mathbb{R}^{n_v} \times \mathbb{R}^{n_\theta}$. This fact is shown in Appendix A by means of a series of auxiliary results. In particular, Lemma 4 shows that the contraction rate is given by $\min\{\alpha, \lambda_1\}$.

It follows that all solutions of (29) starting in $W \times \mathbb{R}^{n_v} \times \mathbb{R}^{n_\theta}$ converge towards each other, exponentially fast, with convergence rate given by $\min\{\alpha, \lambda_1\}$. Since those solutions include $\text{col}(w(t), v(t), \theta(t))$ and $\text{col}(\hat{w}(t), \hat{v}(t), \hat{\theta}(t))$, the result is proven. \square

B. Application to conductance-based models

Theorem 1 applies to any conductance-based model of a neuronal network (Sections II and III). We can see that Proposition 1 guarantees that Assumption 1 is satisfied, while Proposition 2 guarantees that Assumption 2 is satisfied with a constant diagonal $M_1 \succ 0$, $\lambda_1 = \bar{\tau}^{-1}$, and $W = [0, 1]^{n_w}$.

We also stress that in the special case where the estimated parameters only include maximal conductances (as in Example 4), the structure of the observer is de facto distributed, that is, it decouples into n_v independent single-neuron observers. This property is of practical and biological relevance. This is formalized in the following result:

Corollary 1. *Let the system (2) describe a conductance-based network model with the parametrization*

$$\theta = \text{col}(\mu^{(1)}, \dots, \mu^{(n_v)}),$$

where $\mu^{(i)}$ collects the maximal conductances appearing in the dynamics of v_i ($i \in \mathcal{N}$). Consider the n_v independent adaptive observers given by

$$\begin{aligned} \dot{\hat{v}}_i &= \varphi_i(v_i, \hat{w}^{(i)})\hat{\mu}^{(i)} + \frac{1}{c_i}u_i + \gamma(1 + \psi_i P_i \psi_i^\top)(v_i - \hat{v}_i) \\ \dot{\hat{w}}^{(i)} &= g(v, \hat{w}^{(i)}) \\ \dot{\hat{\mu}}^{(i)} &= \gamma P_i \psi_i^\top (v_i - \hat{v}_i) \\ \dot{\psi}_i &= -\gamma \psi_i + \varphi_i(v_i, \hat{w}^{(i)}), \\ \dot{P}_i &= \alpha P_i - P_i \psi_i^\top \psi_i P_i \end{aligned} \quad (30)$$

where $P_i(0) \succ 0$ and $i \in \mathcal{N}$. Let Assumption 3 hold for

$$\Psi(t) = \text{diag}_{i \in \mathcal{N}}(\psi_i(t)) \quad (31)$$

and let $\alpha > 0$ and $\gamma > \min\{\alpha, \bar{\tau}^{-1}, 1\}$, where $\bar{\tau}$ is the time-constant upper bound given by (13). Then, for all $\hat{\mu}(0) \in \mathbb{R}^{n_\mu}$, we have $\hat{\mu}(t) \rightarrow \mu$ exponentially fast as $t \rightarrow \infty$, with a convergence rate given by $\min\{\alpha, \bar{\tau}^{-1}\}$.

Proof. The parametrization for θ implies that

$$\Phi(v, w) = \text{diag}_{i \in \mathcal{N}}\{\varphi_i(v_i, w^{(i)})\}$$

so that, choosing $\Psi(0) = \text{diag}_{i \in \mathcal{N}}(\psi_i(0))$, the matrix Ψ in (22) is given by (31). Choosing $P(0) = \text{diag}_{i \in \mathcal{N}}(P_i(0))$ then we also have $P(t) = \text{diag}_{i \in \mathcal{N}}(P_i(t))$ for all $t \geq 0$; this is most easily seen from the solution $R(t) = P^{-1}(t)$ of (49), which retains the block-diagonal structure of $R(0) = P(0)^{-1}$ and $\Psi^\top \Psi = \text{diag}_{i \in \mathcal{N}}(\psi_i \psi_i^\top)$. Thus we can ignore all off-block

diagonal terms of $\Psi(t)$ and $P(t)$ in the adaptive observer (22), resulting in the observer above. \square

C. Time-varying parameters

In this section, we address the case in which the true parameters $\theta(t)$ are time-varying. This can be modelled according to

$$\dot{v} = \Phi(v, w, u)\theta + b(v, w, u) \quad (32a)$$

$$\dot{w} = g(v, w) \quad (32b)$$

$$\dot{\theta} = d(t, v, w) \quad (32c)$$

where $d(t, v, w)$ governs the trajectories of θ . Now, the state $\text{col}(\hat{v}, \hat{w}, \hat{\theta})$ of the adaptive observer is not guaranteed to converge to the state of (32). However, we can show that the adaptive observer yields online estimates $\hat{\theta}(t)$ that track the time-varying $\theta(t)$ in an approximate sense. More precisely, the estimates will be guaranteed to enter a certain neighbourhood of true parameters as $t \rightarrow \infty$. Similarly to [5], [9], we shall treat the term $d(t, v, w)$ as a disturbance in the dynamics of θ , and use the exponential contraction property of the virtual system (29) to obtain an explicit description of this neighbourhood. We require the following boundedness assumption:

Assumption 4. The solution $\text{col}(v, w, \theta)$ of (32) remains in the compact set $V \times W \times \Theta$ for all $t \geq 0$. Furthermore, for some $\bar{d} > 0$, we have $\|d(t, v, w)\| \leq \bar{d}$ for all $t \geq 0$.

We can now state the following:

Proposition 4. *Let Assumptions 1 to 4 hold, let α and γ be as in Theorem 1, and let $\hat{v}(0) \in \mathbb{R}^{n_v}$, $\hat{w}(0) \in W$, and $\hat{\theta}(0) \in \mathbb{R}^{n_\theta}$. Then, there exist constants $\zeta_1, \ell_\theta > 0$ and a sufficiently small $\varepsilon > 0$ such that the solution $\text{col}(\hat{v}(t), \hat{w}(t), \hat{\theta}(t))$ converges exponentially fast towards the Euclidean ball $\mathcal{B}_\rho(t)$ centred at $\text{col}(v(t), w(t), \theta(t))$ and of constant radius given by*

$$\rho = \left(\frac{\varepsilon}{\lambda \min\{\sigma_1, \varepsilon \zeta_1\}} \left(\|P^{-1}(0)\| + \frac{(\alpha + 1)\ell_\theta^2}{\alpha \gamma^2} \right) \right)^{\frac{1}{2}} \bar{d}$$

where $\lambda = \min\{\alpha, \lambda_1\}$.

Proof. Consider the nominal virtual system

$$\dot{\xi} = f(t, \xi) \quad (33)$$

where $\xi = \text{col}(s, r, \eta)$, and $f(t, \xi)$ is given by the right-hand side of (29). Consider also the perturbed virtual system

$$\dot{\xi}_p = f(t, \xi_p) + f_d(t, \xi_p) \quad (34)$$

where $\xi_p = \text{col}(s_p, r_p, \eta_p)$ and

$$f_d(t, \xi_p) = (0, 0, d(t, r_p, s_p))^\top \quad (35)$$

In Appendix A, we have shown that (33) is exponentially contracting on $W \times \mathbb{R}^{n_v} \times \mathbb{R}^{n_\theta}$, with a contraction metric $M(t)$ given by (56). From [33, Section 3.7 (vii)], this implies that

$$\|\xi_p(t) - \xi(t)\|_{M(t)} \leq e^{-\lambda t} \|\xi_p(0) - \xi(0)\|_{M(0)} + \tilde{f}_d(t) \quad (36)$$

for all $t \geq 0$, with

$$\tilde{f}_d(t) = \int_0^t e^{-\lambda(t-\tau)} \|f_d(\tau, \xi_p(\tau))\|_{M(\tau)} d\tau \quad (37)$$

By Assumption 4, (35), (45), and (56), we have

$$\begin{aligned} \|f_d\|_M^2 &= \varepsilon \|d\|_{P^{-1} + \Psi^T \Psi}^2 \\ &\leq \varepsilon \bar{d}^2 (\|P^{-1}\| + \|\Psi^T \Psi\|) \\ &\leq \varepsilon \bar{d}^2 (\kappa_2 + \ell_\theta^2 / \gamma^2) \end{aligned}$$

for all $t \geq 0$, where in the last inequality we have used (46) and (47)-(48). Thus

$$\tilde{f}_d(t) \leq \varepsilon \bar{d}^2 (\kappa_2 + \ell_\theta^2 / \gamma^2) / \lambda \quad (38)$$

It follows from (36), (38), and (57) that

$$\|\xi_p(t) - \xi(t)\| \leq \frac{\|\xi_p(0) - \xi(0)\|_{M(0)}}{\min\{\sigma_1, \varepsilon \zeta_1\}^{\frac{1}{2}}} e^{-\lambda t} + \rho \quad (39)$$

for all $t \geq 0$, where to obtain ρ we have replaced κ_2 with its value given by (51).

The inequality (39) shows that any solution $\xi(t)$ of the nominal virtual system (33) converges exponentially fast towards the Euclidean ball centred at $\xi_p(t)$ and of constant radius given by ρ , where $\xi_p(t)$ is any solution of the perturbed virtual system (34). Now, let $x(t) := \text{col}(w(t), v(t), \theta(t))$ and $\hat{x}(t) := \text{col}(\hat{w}(t), \hat{v}(t), \hat{\theta}(t))$ be the solutions of (32) and (22), respectively. We have that $x(t)$ is a particular solution of the perturbed virtual system (34). In addition, $\hat{x}(t)$ is a particular solution of the exponentially contracting nominal virtual system (33), and thus it converges exponentially fast towards any other such solution $\xi(t)$. Thus, $\hat{x}(t)$ converges exponentially fast towards $\mathcal{B}_\rho(t)$. \square

Remark 3. Proposition 4 provides a number of insights that are useful to understand the trade-offs involved in tuning the observer adaptation gains:

- i) For small ε , the radius of $\mathcal{B}_\rho(t)$ will be independent of ε , but inversely proportional to ζ_1 , which according to Lemma 3 in Appendix A must satisfy $\zeta_1 < \min\{\kappa_1, 1\}$. Ensuring a large κ_1 is therefore important for the parameter estimates to closely track the true time-varying parameters. Given the expression for κ_1 in (50), this shows the importance of ensuring a persistent excitation through a large δ and a small T . It also shows that one should avoid too large of a forgetting rate α .
- ii) A large γ decreases the radius of $\mathcal{B}_\rho(t)$. Thus, increasing γ is a good strategy if close tracking of time-varying parameters is required. However, too large a value for the gain γ may not be desirable when $v(t)$ is corrupted by noise.
- iii) The stronger the contraction property of the internal dynamics, that is, the larger are σ_1 and λ_1 , the better for the estimation of time-varying parameters.

V. APPLICATIONS IN NEUROPHYSIOLOGY

The design of the adaptive observer in this paper is system theoretic and grounded in the literature of adaptive control, whose results have been primarily applied to robotics

and process control. While the practical significance of this observer for neurophysiology remains to be demonstrated, this section illustrates how it could be used in experimental investigations in that field. The numerical results also illustrate the performance of the algorithm⁴.

A. System identification of biophysical neuronal models

Ion channels have been studied for a long time [20], and online databases such as ModelDB [39] now provide well-documented state-space models for many different types of ionic currents. Thanks to the modularity of conductance-based models, arbitrary model structures can be postulated by connecting in parallel readily available ionic current models with fixed gating variable dynamics. The primary goal of neuronal system identification is then to estimate the remaining unknown model parameters — capacitances, maximal conductances and reversal potentials [8], [14], [24], [40]. In this section, we illustrate a real-time version of this approach by applying the adaptive observer (22)-(23) to the Hodgkin-Huxley model introduced in Example 1 and parameterized as described in Example 3.

In the numerical simulations that follow, we use the original biophysical parameters from Table I, and the gating variable dynamics $g(v, w)$ described in Appendix C.1. According to the lumped parametrization of Example 3, the parameters in Table I result in a constant θ given by

$$\theta = (120, 36, 0.3, 6600, -2772, -16.32, 1)^T$$

We simulated the true HH model and the adaptive observer when they are subject to the input

$$u(t) = \sin(2\pi t/10)$$

for $t \geq 0$. Notice that a non-constant u is in this case a necessary condition for persistent excitation, as otherwise $\Phi(v, w, u)$ contains linearly dependent terms. The initial conditions of the voltage and gating variables are given by

$$(v(0), m_{\text{Na}}(0), h_{\text{Na}}(0), m_K(0)) = (0, 0, 0, 0)$$

$$(\hat{v}(0), \hat{m}_{\text{Na}}(0), \hat{h}_{\text{Na}}(0), \hat{m}_K(0)) = (-60, 0.5, 0.5, 0.5)$$

whereas the remaining initial conditions of the observer are given by $\Psi(0) = 0$, $P(0) = I$, and

$$\hat{\theta}(0) = (60, 60, 10, 0, 0, 0, 0)^T$$

For $\alpha = 0.5$ and $\gamma = 5$, the solutions of the true system and of the adaptive observer can be seen in Figure 5. All the parameter estimates of the adaptive observer converge to the true parameter values.

B. Neuromodulation studies

Neuromodulators continuously modulate the opening of ion channels in a neuron's membrane. This modulatory control can be modelled as a temporal variation of the maximal conductances in a conductance-based model [13]. Many neuromodulation studies have focused on small networks governing

⁴The Julia code used to generate these results can be found on <https://github.com/thiagoburghi/online-learning>.

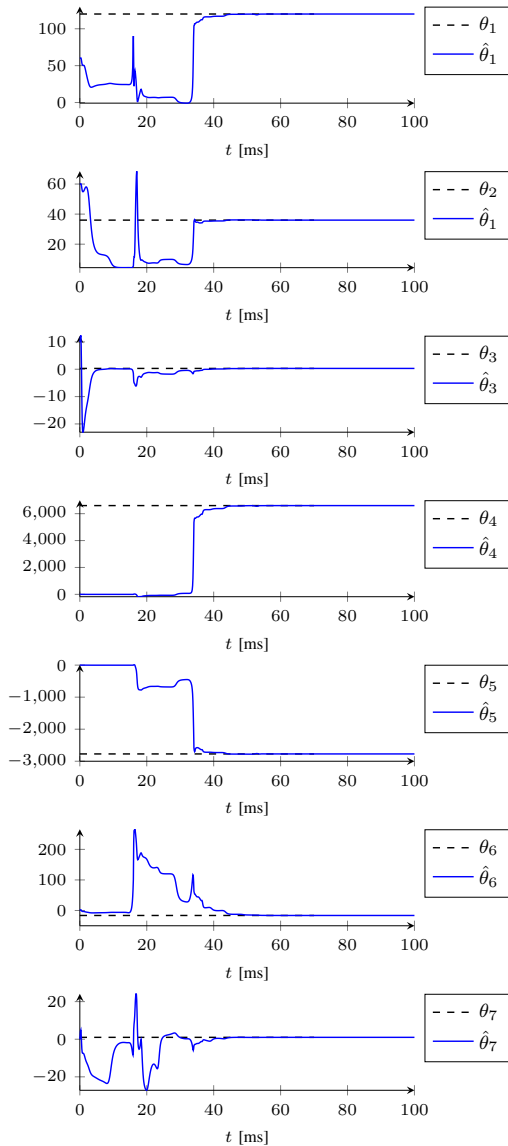


Fig. 5. Trajectories of the true parameters and estimated parameters of the adaptive observer (22)-(23) in the estimation of the HH model introduced in Example 1 and parameterized as in Example 3.

elementary animal rhythmic functions [18], [38]. A simple example is the modulation of the half-center oscillator model presented in Example 2. It is well-known [10] that the bursting rhythm of each neuron in this model can be controlled by modulating the Calcium maximal conductances $\mu_{Ca,1}(t)$ and $\mu_{Ca,2}(t)$. We simulate such a scenario and use the adaptive observer (30) to estimate all maximal conductances of the model.

A gradual increase in the concentration of calcium ion channels is simulated in both neurons according to

$$\mu_{Ca(t),1}(t) = \mu_{Ca,2}(t) = 0.1 + \frac{0.06}{1 + \exp\left(-\frac{t-T_f/2}{1250}\right)} \quad (40)$$

where $T_f = 15$ seconds is the length of the simulation. In Table II, we list the remaining maximal conductances of the HCO model used in this simulation. In Appendix C.2, we detail its reversal potentials and capacitances, as well as its

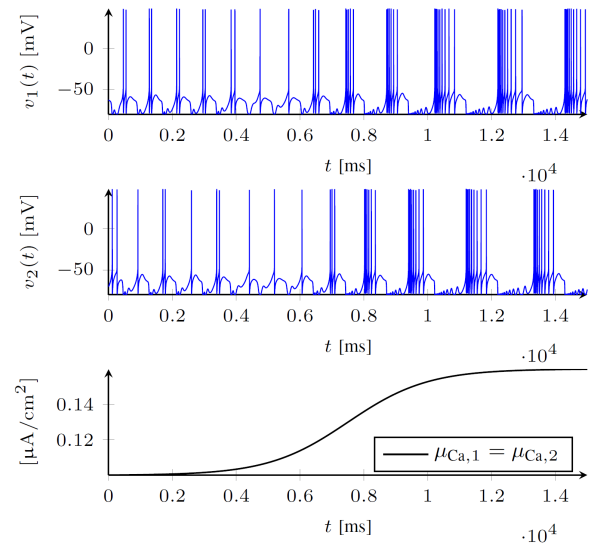


Fig. 6. True HCO voltage traces and time-varying calcium conductance used in Section V-B.

internal dynamics vector field $g(v, w)$.

Figure 6 illustrates the resulting voltage traces of the HCO. Notice the neuromodulatory action on the calcium conductance increases the number of spikes and duty-cycle of each burst.

For a forgetting rate of $\alpha = 0.01$, an observer gain of $\gamma = 10$, and a constant input $u_1(t) = u_2(t) = -0.65 \mu\text{A}/\text{cm}^2$, Figure 7 shows the trajectories of some of the maximal conductance estimates compared to the true system maximal conductances (the behavior of the omitted estimates is similar). For the initial conditions used in this simulation, see Appendix D. It can be seen that, whenever the calcium conductances are varying slowly, the estimates converge to a very small interval (not distinguishable in the figure) around the true parameter values. Towards the middle of the simulation, when the calcium conductances are varying more rapidly, the estimates deviate more visibly from the true parameter values; however the estimates still track these values in an approximate sense. A comparison with Figure 6 shows that estimates are corrected whenever a burst of spikes is elicited. Each burst can thus be seen as providing a very rich signal for the observer to update its estimates. Consistently with the analysis of Section IV-C, this behaviour demonstrates the robustness of the adaptive observer to unmodelled parameter dynamics.

C. Adaptive control of a bursting behaviour

The idea of controlling a biological neuron became a reality ever since the development of the *dynamic clamp* technique

TABLE II
HCO MAXIMAL CONDUCTANCES USED IN SECTION V-B ($i = 1, 2$).

$\mu_{Na,i}$	$\mu_{K,i}$	$\mu_{Ca,i}$	$\mu_{L,i}$	$\mu_{G,2,1}$	$\mu_{G,1,2}$
60	40	see (40)	0.035	4	4

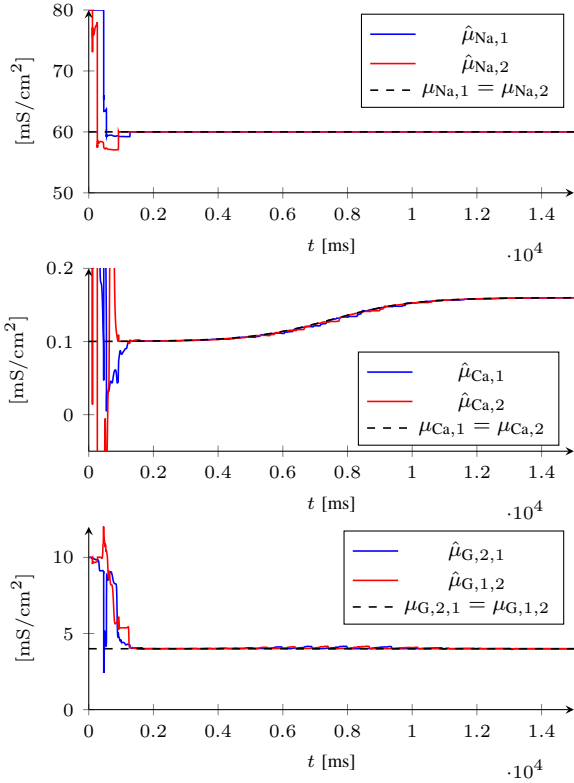


Fig. 7. Trajectories of maximal conductance estimates for the HCO described in Section V-B.

[48]. In dynamic clamp experiments, artificial ionic currents are added to a biological neuron by designing an appropriate control law for the input current. This can be explored, for instance, to study the reliability of neuronal behavior to neuromodulation [19]. Conceptually, dynamic clamp is made possible by the structure of (2a)-(2b), which is particularly suitable for adding new currents, or modifying the maximal conductance of existing ones. More technically, (2a)-(2b) is in global norm form [25], and thus its dynamics can be reshaped by means of output feedback.

In this section, we show that it is possible to use parameter estimates from the adaptive observer in order to *adaptively* control a neuron whose biophysical parameters are initially unknown. This is the essence of *indirect adaptive control* schemes [2, Chapter 3], where controller parameters are continuously updated based on an estimated model of the plant. As an example, we show how the burst length of a rebound burster neuron with unknown parameters can be controlled using the adaptive observer of Section IV. A rebound burster is a neuron that responds to an inhibitory pulse of input current with a burst of spikes [10]. A simple rebound burster can be obtained by isolating one of the neurons in the HCO of Example 2, and removing its synaptic connections. The voltage dynamics of this rebound burster are thus given by

$$c\dot{v} = -\mu_{\text{Na}}m_{\text{Na}}^3h_{\text{Na}}(v - \nu_{\text{Na}}) - \mu_{\text{K}}m_{\text{K}}^4(v - \nu_{\text{K}}) - \mu_{\text{Ca}}m_{\text{Ca}}^3h_{\text{Ca}}(v - \nu_{\text{Ca}}) - \mu_{\text{L}}(v - \nu_{\text{L}}) + u \quad (41)$$

In this example, the true maximal conductances and the capacitance are given in Table III, whereas the reversal potentials and

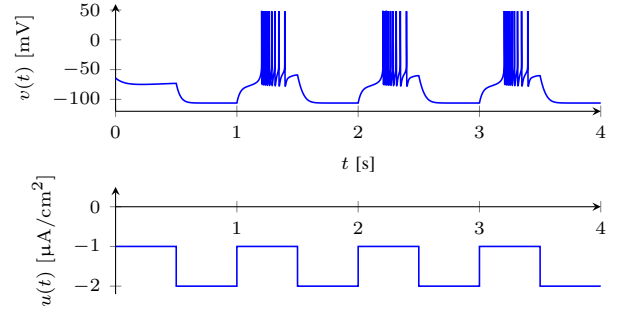


Fig. 8. Open-loop behaviour of the rebound burster neuron of Section V-C. Top: membrane voltage. Bottom: input applied current.

internal dynamics are again detailed in Appendix C.2. Using these parameters, we obtain the rebound bursting behavior seen in Figure 8.

TABLE III

REBOUND BURSTER BIOPHYSICAL PARAMETERS USED IN SECTION V-C.

μ_{Na}	μ_{K}	μ_{Ca}	μ_{L}	c
60	40	0.18	0.035	1

The model (41) can be thought of as representing a biological neuron with constant unknown maximal conductances. Suppose we wish to control this neuron so that it responds to the input of Figure 8 with shorter bursts. To control the duration of a burst, we need to be able to change its calcium conductance μ_{Ca} (cf. Figure 6). Assuming knowledge of reversal potentials, this can be achieved by implementing the control law

$$u = -(\bar{\mu}_{\text{Ca}} - \hat{\mu}_{\text{Ca}})\hat{m}_{\text{Ca}}^3\hat{h}_{\text{Ca}}(v - \nu_{\text{Ca}}) + \bar{u} \quad (42)$$

where $\bar{\mu}_{\text{Ca}}$ is a desired calcium maximal conductance (chosen to produce a desired burst length), \bar{u} is a closed-loop input signal, and $\hat{\mu}_{\text{Ca}}$, \hat{m}_{Ca}^3 , and \hat{h}_{Ca} are estimates obtained with the adaptive observer (30). Here, we do not discuss the design of the desired constant $\bar{\mu}_{\text{Ca}}$, but we remark that in principle it may depend on other maximal conductance estimates (see [44], [47] for design principles of bursting behaviors).

Notice that although (42) effectively closes the loop between the adaptive observer and the true system, the proof of Theorem 1 still holds, as the term $u(t)$ merely appears as a time-varying term in the virtual system (29). Thus our convergence analysis guarantees that $(\hat{\mu}_{\text{Ca}}, \hat{m}_{\text{Ca}}, \hat{h}_{\text{Ca}}) \rightarrow (\mu_{\text{Ca}}, m_{\text{Ca}}, h_{\text{Ca}})$ as $t \rightarrow \infty$, and the neuron will asymptotically produce the desired behavior due to the choice of $\bar{\mu}_{\text{Ca}}$. Notice also that a much more general feedback law $u(t)$ modifying all the maximal conductances of (41) could have been used; we limit ourselves to the feedback law (42) for didactic purposes.

For a desired $\bar{\mu}_{\text{Ca}} = 0.125$, Figure 9 shows the behavior of key variables of the the closed-loop system given by the controlled rebound burster with voltage dynamics (41) under the adaptive feedback law given by (30) and (42). It can be seen that while the estimate $\hat{\mu}_{\text{Ca}}$ is far from the true μ_{Ca} (in

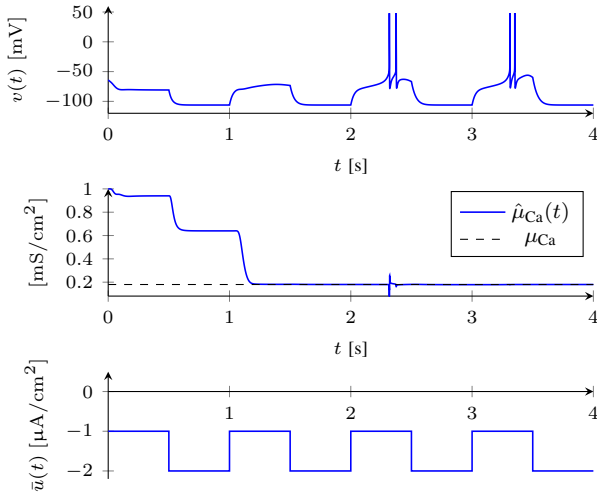


Fig. 9. Closed-loop behaviour of the rebound burster neuron of Section V-C for a desired $\bar{\mu}_{Ca} = 0.125$. Top: voltage of the controlled neuron. Middle: calcium conductance estimate (solid) and true value (dashed). Bottom: closed-loop input.

the time interval $t < 1200$ ms), the controlled neuron does not burst after the first inhibitory input pulse. After $\hat{\mu}_{Ca}$ has settled, the neuron bursts with a much shorter burst length than the one observed in open-loop (Figure 8). Thus the objective of the adaptive control law is achieved.

VI. CONCLUSION AND FURTHER WORK

We have presented an adaptive observer which can be used for real-time estimation of conductance-based models of neuronal networks. The key properties of this model class are uniformly exponentially contracting internal dynamics and the existence of a positively invariant set in the state-space.

There are several directions for future work. First, we have not addressed the estimation of parameters in the internal dynamics (2b). For conductance-based models, this is a difficult problem, as their internal dynamics depends nonlinearly on these parameters. In future work, we will address this issue by performing real-time estimation of conductance-based models using a universal approximator for the internal dynamics, as in [7].

It is also worth commenting that the adaptive observer (30) possesses features which are desirable from the biological point of view. In particular, the update rule for maximal conductances of the i^{th} neuron is *local* [4] — it depends only on the voltage of that neuron, and (through the synaptic gating variables) on the voltages of neurons that are presynaptic to it. Thus, another direction for future work is concerned with the physiological plausibility of adaptive observers derived from system theoretic properties, in particular in comparison with online estimation schemes such as those studied in [4], [6], [27].

APPENDIX

A. Contraction of the virtual system (29)

To begin, notice that, in (29), we have swapped the first two equations relative to those of the true system and the

adaptive observer. This was done to emphasize the system structure: the subsystem (29a) with output s is in a series connection with the subsystem (29b)–(29c) with input s . To show that the virtual system is exponentially contracting on $W \times \mathbb{R}^{n_v} \times \mathbb{R}^{n_\theta}$, we will exploit this structure. The main idea is to ensure that (29b)–(29c) is globally exponentially contracting, uniformly in s on \mathbb{R}^{n_w} . As we shall see, that is the purpose of using the function $a(t, s, \eta)$ in the definition of (29b). Once this is ensured, then showing contraction of the whole virtual system (29) becomes simple, as the dynamics (29a) are already exponentially contracting by Assumption 2. In what follows, we prove each of these contraction results separately. For that purpose, we write the *differential* virtual system as

$$\begin{pmatrix} \dot{\delta s} \\ \dot{\delta r} \\ \dot{\delta \eta} \end{pmatrix} = \underbrace{\begin{bmatrix} J_{1,1} & 0 \\ J_{2,1} & J_{2,2} \end{bmatrix}}_J \begin{pmatrix} \delta s \\ \delta r \\ \delta \eta \end{pmatrix} \quad (43)$$

where the block entries in the Jacobian J above are given by

$$\begin{aligned} J_{1,1} &= \partial_s g(v, s), \\ J_{2,1} &= \begin{bmatrix} \partial_s (\Phi(v, s, u)\theta + b(v, s, u)) \\ 0 \end{bmatrix}, \\ J_{2,2} &= \begin{bmatrix} -\gamma(I + \Psi P \Psi^\top) & \Phi(v, \hat{w}, u) \\ -\beta P \Psi^\top & 0 \end{bmatrix} \end{aligned} \quad (44)$$

In the remainder of this section, we always assume Assumptions 1 and 3 hold.

1) *Contraction of the virtual subsystem (29b)–(29c)*: We first show that a simple condition on the gain γ ensures that the virtual subsystem (29b)–(29c) is globally exponentially contracting, uniformly in s , with a uniformly positive definite and bounded contraction metric given by

$$M_2 = \begin{bmatrix} I & -\Psi \\ -\Psi^\top & P^{-1} + \Psi^\top \Psi \end{bmatrix} \quad (45)$$

where we have omitted the time arguments for clarity. To begin, we need to show that P^{-1} exists, and also verifies those properties. To that end, we make use of the following simple fact:

Lemma 1. *We have*

$$\|\Psi(t)\| \leq \frac{\ell_\theta}{\gamma} \quad (46)$$

for all $t \geq 0$ and some constant $\ell_\theta > 0$.

Proof. This follows from the solution of (23a), given by

$$\Psi(t) = \int_0^t e^{-\gamma(t-\tau)} \Phi(v(\tau), \hat{w}(\tau), u(\tau)) d\tau$$

Since Φ is continuous and $\{v, \hat{w}, u\}$ remains in the compact set $Y \times W \times U$, there exists a constant $\ell_\theta > 0$ such that

$$\begin{aligned} \|\Psi(t)\| &\leq \int_0^t e^{-\gamma(t-\tau)} \|\Phi(v(\tau), \hat{w}(\tau), u(\tau))\| d\tau \\ &\leq \ell_\theta \int_0^t e^{-\gamma(t-\tau)} d\tau \end{aligned}$$

for all $t \geq 0$. Evaluating the integral then yields (46). \square

We can now show P can be inverted, and its inverse is uniformly positive definite and bounded:

Lemma 2. *The matrix $P(t)$ is invertible for all $t \geq 0$, and*

$$R(t) := P(t)^{-1} \quad (47)$$

satisfies

$$\kappa_1 I \preceq R(t) \preceq \kappa_2 I \quad (48)$$

for all $t \geq 0$ and some constants $\kappa_1 > 0$ and $\kappa_2 > 0$.

Proof. The result follows from analyzing the solution of the system

$$\dot{R} = -\alpha R + \Psi^\top \Psi \quad (49)$$

with $R(0) = P(0)^{-1} \succ 0$. To obtain the lower bound $\kappa_1 I$, we make use of Assumption 3 and follow the same steps as in the proof of [59, Lemma 1], which yields

$$\kappa_1 = \min \{ \lambda_{\min} [e^{-\alpha T} R(0)], \delta e^{-2\alpha T} \} \quad (50)$$

To obtain the upper bound $\kappa_2 I$, we bound the solution of (49) according to

$$\|R(t)\| \leq \|R(0)\| + \int_0^t e^{-\alpha(t-\tau)} \|\Psi(\tau)\|^2 d\tau$$

where we have used the identity $\|\Psi(\tau)^\top \Psi(\tau)\| = \|\Psi(\tau)\|^2$. Thus it follows from Lemma 1 that $\|R(t)\| \leq \kappa_2$, with

$$\kappa_2 = \|R(0)\| + \frac{\ell_\theta^2}{\alpha \gamma^2} \quad (51)$$

This implies $R(t)$ is invertible for all $t \geq 0$, and thus so is $P(t) := R(t)^{-1}$. We can see $P(t)$ is a solution of (23b) by using the identity $\dot{R} = \dot{P}^{-1} = -P^{-1} \dot{P} P^{-1}$ in (49). \square

Now, we address the contraction property of the subsystem (29b)–(29c). To do so, let

$$Q_2 = J_{2,2}^\top M_2 + M_2 J_{2,2} + \dot{M}_2 \quad (52)$$

with $J_{2,2}$ given by (44) and M_2 given by (45). Then we have the following.

Lemma 3. *Let $\gamma > \alpha$. Then*

$$Q_2 \preceq -\alpha M_2 + \begin{bmatrix} -\gamma I & 0 \\ 0 & -(\gamma - 1) \Psi^\top \Psi \end{bmatrix} \quad (53)$$

for all $\{r, \eta\} \in \mathbb{R}^{n_v} \times \mathbb{R}^{n_\theta}$, all $s \in \mathbb{R}^{n_w}$, and all $t \geq 0$. Furthermore, there exist positive constants $\zeta_1 < \min\{1, \kappa_1\}$ and $\zeta_2 > \max\{1, \kappa_2\}$ such that

$$\zeta_1 I \leq M_2 \leq \zeta_2 I \quad (54)$$

for all $t \geq 0$.

Proof. To show (53), we compute Q_2 , obtaining

$$Q_2 = \begin{bmatrix} -\gamma I & \gamma \Psi \\ \gamma \Psi^\top & -\alpha P^{-1} - \gamma \Psi^\top \Psi \end{bmatrix} + \begin{bmatrix} -\gamma I & 0 \\ 0 & (1 - \gamma) \Psi^\top \Psi \end{bmatrix}$$

where we have used (47)–(49) to compute \dot{M}_2 .

Now, since $\gamma > \alpha$, Lemma 5 in Appendix B (Schur's complement) can be used to show that

$$\begin{bmatrix} -\gamma I & \gamma \Psi \\ \gamma \Psi^\top & -\alpha P^{-1} - \gamma \Psi^\top \Psi \end{bmatrix} + \alpha M_2 \preceq 0$$

which implies the inequality (53).

To show the lower bound in (54), we use Lemma 5 again to see that $M_2 - \zeta_1 I \succeq 0$ if and only if

$$P^{-1} - \zeta_1 I - \frac{\zeta_1}{1 - \zeta_1} \Psi^\top \Psi \succeq 0 \quad (55)$$

But using the upper bound of Ψ from Lemma 1 and the lower bound of P^{-1} from Lemma 2, we have

$$P^{-1} - \zeta_1 I - \frac{\zeta_1}{1 - \zeta_1} \Psi^\top \Psi \succeq \left(\kappa_1 - \zeta_1 - \frac{\zeta_1}{1 - \zeta_1} \frac{\ell_\theta^2}{\gamma^2} \right) I$$

It is clear, by continuity of the right-hand side of the inequality above in ζ_1 , that (55) will be satisfied if we choose a sufficiently small ζ_1 with $0 < \zeta_1 < \min\{1, \kappa_1\}$. Thus there is a ζ_1 such that $M_2 \succeq \zeta_1 I$ as claimed. A similar analysis shows that $\zeta_2 I \succeq M_2$ for a sufficiently large $\zeta_2 > \max\{1, \kappa_2\}$. \square

2) Contraction of the virtual system (29): It follows directly from Lemma 3 that for any $\gamma > \min\{\alpha, 1\}$ and all $t \geq 0$, the subsystem (29b)–(29c) is globally exponentially contracting, uniformly in s . In this case, since (29b)–(29c) is connected in series with the contracting subsystem (29a), we follow [49, Section 3.2] and show contraction of the full virtual system (29) using the metric

$$M(t) = \begin{bmatrix} M_1(t) & 0 \\ 0 & \varepsilon M_2(t) \end{bmatrix} \quad (56)$$

where M_1 is the contraction metric of Assumption 2, M_2 is given by (45), and $\varepsilon > 0$ is an arbitrary constant. To do so, let

$$Q = MJ + J^\top M + \dot{M}$$

where J is given by (43)–(44). Computing Q , we obtain

$$Q = \begin{bmatrix} Q_1 & \varepsilon J_{2,1}^\top M_2 \\ \varepsilon M_2 J_{2,1} & \varepsilon Q_2 \end{bmatrix}$$

where Q_1 is given by (27), and Q_2 is given by (52). Since Q_1 and Q_2 are negative definite according to the inequalities (28) and (53), respectively, we are able to show contraction of the virtual system by choosing a small ε :

Lemma 4. *Let*

$$\lambda = \min\{\alpha, \lambda_1\}$$

and $\gamma > \min\{\alpha, \lambda_1, 1\}$. Then, there exist constants $\zeta_1, \zeta_2 > 0$ and a sufficiently small $\varepsilon > 0$ such that

$$\text{diag}(\sigma_1 I, \varepsilon \zeta_1 I) \preceq M(t) \preceq \text{diag}(\sigma_2 I, \varepsilon \zeta_2 I) \quad (57)$$

and

$$Q \preceq -\lambda M \quad (58)$$

for all $\{s, r, \eta\} \in W \times \mathbb{R}^{n_v} \times \mathbb{R}^{n_\theta}$ and all $t \geq 0$.

Proof. The matrix inequalities in (57) follow from (26) and Lemma 3. To verify (58), we apply Lemma 5 in Appendix B to check positive semidefiniteness of $-(Q + \lambda M)$. From Assumption 2, we have

$$Q_1 + \lambda M_1 \preceq -\lambda_1 M_1 \preceq -\lambda_1 \sigma_1 I \quad (59)$$

and so by uniform positive definiteness of $-(Q_1 + \lambda M_1)$ it follows that $-(Q + \lambda M) \succeq 0$ if and only if

$$-(Q_2 + \lambda M_2) + \varepsilon M_2 J_{2,1} (Q_1 + \lambda M_1)^{-1} J_{2,1}^T M_2 \succeq 0$$

Using the fact that $\lambda \leq \alpha$, as well as (59), we see that a sufficient condition for the above inequality to be satisfied is

$$-(Q_2 + \alpha M_2) - \varepsilon \frac{1}{\lambda_1 \sigma_1} M_2 J_{2,1} J_{2,1}^T M_2 \succeq 0 \quad (60)$$

Now since $\{v(t), u(t)\}$ belongs to the compact set $V \times U$ for all $t \geq 0$, and since θ is constant, it is clear from (44) that $J_{2,1}$ is bounded as long as $s \in W$, where W is also compact. More precisely, there exists a constant $\ell_s > 0$ such that

$$J_{2,1} J_{2,1}^T \preceq \begin{bmatrix} \ell_s^2 I & 0 \\ 0 & 0 \end{bmatrix} \quad (61)$$

for all $t \geq 0$ and all $s \in W$.

Using (53) and (61), we see that (60) holds for all $t \geq 0$ and all $s \in W$ if

$$\begin{bmatrix} \gamma & 0 \\ 0 & (\gamma - 1) \Psi^T \Psi \end{bmatrix} - \varepsilon \frac{\ell_s^2}{\lambda_1 \sigma_1} \begin{bmatrix} I & -\Psi \\ -\Psi^T & \Psi^T \Psi \end{bmatrix} \succeq 0 \quad (62)$$

Since $\gamma > 1$, it is easy to see (for instance, by Lemma 5) that (62) holds for sufficiently small $\varepsilon > 0$. \square

B. Supporting results

Lemma 5 (Schur's complement [57]). *Let X be a real symmetric matrix given by*

$$X = \begin{bmatrix} A & B \\ B^T & C \end{bmatrix}$$

Then $X \succ 0$ if and only if $A \succ 0$ and $C - B^T A^{-1} B \succ 0$; if $A \succ 0$, then $X \succeq 0$ if and only if $C - B^T A^{-1} B \succeq 0$. Alternatively, $X \succ 0$ if and only if $C \succ 0$ and $A - B C^{-1} B^T \succ 0$; if $C \succ 0$, then $X \succeq 0$ if and only if $A - B C^{-1} B^T \succeq 0$.

C. Model parameters

1) *Hodgkin-Huxley model*: HH model parameters were adapted from [26, pp. 46-47]. The activation functions are of the form (5), and the time-constant functions are of the form

$$\tau(v) = c_{\text{base}} + c_{\text{camp}} \exp\left(-\frac{(v - c_{\text{mean}})^2}{c_{\text{std}}^2}\right) \quad (63)$$

with parameters given in Table IV.

TABLE IV

PARAMETERS OF THE ACTIVATION FUNCTIONS (5) AND TIME-CONSTANT FUNCTIONS (63) OF THE HH MODEL USED IN THE PAPER.

	ρ	κ	c_{base}	c_{camp}	c_{mean}	c_{std}
m_{Na}	-40	9	0.04	0.46	-38	30
h_{Na}	-62	-7	1.2	7.4	-67	20
m_{K}	-53	15	1.1	4.7	-79	50

TABLE V

HCO PARAMETERS USED IN SECTIONS V-B AND V-C.

ν_{Na}	ν_{K}	ν_{Ca}	ν_{G}	ν_{L}	c_1	c_2
50	-80	120	-49	-80	1	1

2) *Half-center oscillator and rebound burster*: Both neurons in the HCO of Section V-B, as well as the rebound burster of Section V-C, have identical capacitances, reversal potentials and internal dynamics (with the exception of synaptic current variables, which are absent in the rebound burster). Reversal potentials and capacitances are given in Table V. The internal dynamics were adapted from [10, p.2474]. Intrinsic and synaptic activation functions are of the form (5), with parameters given in Table VI. The time-constant functions $\tau_{m,\text{Na}}$, $\tau_{m,\text{K}}$, $\tau_{m,\text{Ca}}$, and $\tau_{h,\text{Ca}}$, are of the form

$$\tau(v) = c_{\text{base}} + \frac{c_{\text{camp}}}{1 + \exp(-(v - c_{\text{half}})/c_{\text{slope}})} \quad (64)$$

with parameters also given in Table VI, whereas $\tau_{h,\text{Na}}$ is given by

$$\tau_{h,\text{Na}}(v) = 0.67 \frac{1}{1 + e^{-\frac{v+62.9}{10}}} \left(1.5 + \frac{1}{1 + e^{\frac{v+34.9}{3.6}}}\right)$$

Finally, in the synaptic time-constant function (7), $a_{\text{G}} = 2$ and $b_{\text{G}} = 0.1$.

TABLE VI

PARAMETERS OF THE ACTIVATION FUNCTIONS (5) AND TIME-CONSTANT FUNCTIONS (64) OF THE HCO AND REBOUND BURSTER MODELS.

	ρ	κ	c_{base}	c_{camp}	c_{half}	c_{slope}
m_{Na}	-35.5	5.29	1.32	-1.26	-120	25
h_{Na}	-48.9	-5.18	-	-	-	-
m_{K}	-12.3	11.8	7.2	-6.4	-28.3	19.2
m_{Ca}	-67.1	7.2	43.4	-42.6	-68.1	20.5
h_{Ca}	-82.1	-5.5	140	-100	-55	16.9
s_{G}	-45	2	-	-	-	-

D. Simulation initial conditions

In Section V-B, we have chosen the HCO initial conditions $v(0)$ and $w(0)$ from the trajectory observed at steady-state oscillations with $\mu_{\text{Ca}} = 0.1$. The adaptive observer initial conditions were arbitrarily set to $\hat{v}(0) = (-50, -50)^T$, $\hat{w}^{(1)}(0) = \hat{w}^{(2)}(0) = 0$, $\hat{\mu}_{\text{Na},1}(0) = \hat{\mu}_{\text{Na},2}(0) = 80$, $\hat{\mu}_{\text{K},1}(0) = \hat{\mu}_{\text{K},2}(0) = 80$, $\hat{\mu}_{\text{Ca},1}(0) = \hat{\mu}_{\text{Ca},2}(0) = 1$, $\hat{\mu}_{\text{L},1}(0) = \hat{\mu}_{\text{L},2}(0) = 1$, $\hat{\mu}_{\text{G},2,1}(0) = \hat{\mu}_{\text{G},1,2}(0) = 10$, $\psi^{(1)}(0) = \psi^{(2)}(0) = 0$, and $P^{(1)}(0) = P^{(2)}(0) = I$. The observer initial conditions used in Section V-C are identical (except for the absent synaptic conductance) to those detailed above.

REFERENCES

- [1] Henry D. I. Abarbanel, Daniel R. Creveling, and James M. Jeanne. Estimation of parameters in nonlinear systems using balanced synchronization. *Physical Review E*, 77(1), January 2008.
- [2] Karl Johan Åström and Björn Wittenmark. *Adaptive Control*. Dover Publications, Mineola, NY, 2nd edition, January 2008.

- [3] Gildas Besançon. Remarks on nonlinear adaptive observer design. *Systems & Control Letters*, 41(4):271–280, November 2000.
- [4] Rafal Bogacz. A tutorial on the free-energy framework for modelling perception and learning. *Journal of Mathematical Psychology*, 76:198–211, February 2017.
- [5] Silvere Bonnabel and Jean-Jacques Slotine. A Contraction Theory-Based Analysis of the Stability of the Deterministic Extended Kalman Filter. *IEEE Transactions on Automatic Control*, 60(2):565–569, February 2015.
- [6] Christopher L. Buckley, Chang Sub Kim, Simon McGregor, and Anil K. Seth. The free energy principle for action and perception: A mathematical review. *Journal of Mathematical Psychology*, 81:55–79, December 2017.
- [7] Thiago B. Burghi, Maarten Schoukens, and Rodolphe Sepulchre. System identification of biophysical neuronal models. In *59th IEEE Conference on Decision and Control*, pages 6180–6185, Jeju Island, Republic of Korea, December 2020.
- [8] Thiago B. Burghi, Maarten Schoukens, and Rodolphe Sepulchre. Feedback identification of conductance-based models. *Automatica*, 123:109297, January 2021.
- [9] Domitilla Del Vecchio and Jean-Jacques E. Slotine. A Contraction Theory Approach to Singularly Perturbed Systems. *IEEE Transactions on Automatic Control*, 58(3):752–757, March 2013.
- [10] Julie Dethier, Guillaume Drion, Alessio Franci, and Rodolphe Sepulchre. A positive feedback at the cellular level promotes robustness and modulation at the circuit level. *Journal of Neurophysiology*, 114(4):2472–84, October 2015.
- [11] G. Drion, T. O’Leary, J. Dethier, A. Franci, and R. Sepulchre. Neuronal behaviors: A control perspective. In *54th IEEE Conference on Decision and Control*, pages 1923–1944, December 2015.
- [12] Guillaume Drion, Julie Dethier, Alessio Franci, and Rodolphe Sepulchre. Switchable slow cellular conductances determine robustness and tunability of network states. *PLOS Computational Biology*, 14(4):e1006125, April 2018.
- [13] Guillaume Drion, Alessio Franci, and Rodolphe Sepulchre. Cellular switches orchestrate rhythmic circuits. *Biological Cybernetics*, 113(1):71–82, April 2019.
- [14] Shaul Druckmann, Yoav Banitt, Albert Gidon, Felix Schürmann, Henry Markram, and Idan Segev. A Novel Multiple Objective Optimization Framework for Constraining Conductance-Based Neuron Models by Experimental Data. *Frontiers in Neuroscience*, 1(1):7–18, October 2007.
- [15] G. Bard Ermentrout and David H. Terman. *Mathematical Foundations of Neuroscience*. Springer, New York, 2010.
- [16] M. Farza, M. M’Saad, T. Maatoug, and M. Kamoun. Adaptive observers for nonlinearly parameterized class of nonlinear systems. *Automatica*, 45(10):2292–2299, October 2009.
- [17] J.P. Gauthier, H. Hammouri, and S. Othman. A simple observer for nonlinear systems applications to bioreactors. *IEEE Transactions on Automatic Control*, 37(6):875–880, June 1992.
- [18] Jorge Golowasch. Neuromodulation of central pattern generators and its role in the functional recovery of central pattern generator activity. *Journal of Neurophysiology*, 122(1):300–315, July 2019.
- [19] Rachel Grashow, Ted Brookings, and Eve Marder. Reliable neuromodulation from circuits with variable underlying structure. *Proceedings of the National Academy of Sciences*, 106(28):11742–11746, July 2009.
- [20] Bertil Hille. *Ionic channels of excitable membranes*. Sinauer Associates, Sunderland, MA, 1984.
- [21] A. L. Hodgkin and A. F. Huxley. A quantitative description of membrane current and its application to conduction and excitation in nerve. *The Journal of Physiology*, 117(4):500–544, August 1952.
- [22] A. L. Hodgkin, A. F. Huxley, and B. Katz. Measurement of current-voltage relations in the membrane of the giant axon of Loligo. *The Journal of Physiology*, 116(4):424–448, April 1952.
- [23] Guosong Hong and Charles M. Lieber. Novel electrode technologies for neural recordings. *Nature reviews. Neuroscience*, 20(6):330–345, June 2019.
- [24] Quentin J. M. Huys, Misha B. Ahrens, and Liam Paninski. Efficient Estimation of Detailed Single-Neuron Models. *Journal of Neurophysiology*, 96(2):872–890, August 2006.
- [25] Alberto Isidori. *Nonlinear Control Systems*. Communications and Control Engineering. Springer-Verlag, London, 3 edition, 1995.
- [26] Eugene M. Izhikevich. *Dynamical Systems in Neuroscience*. MIT Press, Cambridge, MA, 2007.
- [27] Jannes Jegminat and Jean-Pascal Pfister. Learning as filtering: implications for spike-based plasticity. *arXiv:2008.03198 [q-bio]*, August 2020.
- [28] Jerome Jouffroy and Thor I. Fossen. A Tutorial on Incremental Stability Analysis using Contraction Theory. 31(3):93–106, July 2010.
- [29] James Keener and James Sneyd. *Mathematical Physiology*, volume 8/1. Springer, New York, NY, 2 edition, 2009.
- [30] Daniele Linaaro and Michele Giugliano. Markov Models of Ion Channels. In Dieter Jaeger and Ranu Jung, editors, *Encyclopedia of Computational Neuroscience*, pages 1–14. Springer, New York, NY, 2014.
- [31] L. Ljung. Convergence analysis of parametric identification methods. *IEEE Transactions on Automatic Control*, 23(5):770–783, October 1978.
- [32] Lennart Ljung. *System Identification: Theory for the User*. Prentice Hall PTR, Upper Saddle River, NJ, 1999.
- [33] Winfried Lohmiller and Jean-Jacques E. Slotine. On Contraction Analysis for Non-linear Systems. *Automatica*, 34(6):683–696, June 1998.
- [34] Brett T. Lopez and Jean-Jacques E. Slotine. Adaptive Nonlinear Control With Contraction Metrics. *IEEE Control Systems Letters*, 5(1):205–210, January 2021.
- [35] Andres M. Lozano, Nir Lipsman, Hagai Bergman, Peter Brown, Stephan Chabardes, Jin Woo Chang, Keith Matthews, Cameron C. McIntyre, Thomas E. Schlaepfer, Michael Schuller, Yasin Temel, Jens Volkmann, and Joachim K. Krauss. Deep brain stimulation: current challenges and future directions. *Nature Reviews Neurology*, 15:148–160, March 2019.
- [36] I. R. Manchester, M. M. Tobenkin, and J. Wang. Identification of nonlinear systems with stable oscillations. In *2011 50th IEEE Conference on Decision and Control and European Control Conference*, pages 5792–5797, Orlando, FL, December 2011.
- [37] Eve Marder and Dirk Bucher. Central pattern generators and the control of rhythmic movements. *Current Biology*, 11(23):R986–R996, November 2001.
- [38] Eve Marder, Timothy O’Leary, and Sonal Shruti. Neuromodulation of Circuits with Variable Parameters: Single Neurons and Small Circuits Reveal Principles of State-Dependent and Robust Neuromodulation. *Annual Review of Neuroscience*, 37(1):329–346, 2014.
- [39] Robert A. McDougal, Thomas M. Morse, Ted Carnevale, Luis Marenco, Rixin Wang, Michele Migliore, Perry L. Miller, Gordon M. Shepherd, and Michael L. Hines. Twenty years of ModelDB and beyond: building essential modeling tools for the future of neuroscience. *Journal of Computational Neuroscience*, 42(1):1–10, February 2017.
- [40] C. Daniel Meliza, Mark Kostuk, Hao Huang, Alain Nogaret, Daniel Margoliash, and Henry D. I. Abarbanel. Estimating parameters and predicting membrane voltages with conductance-based neuron models. *Biological Cybernetics*, 108(4):495–516, August 2014.
- [41] Luis Fernando Nicolas-Alonso and Jaime Gomez-Gil. Brain Computer Interfaces, a Review. *Sensors*, 12(2):1211–1279, January 2012.
- [42] Alain Nogaret, C. Daniel Meliza, Daniel Margoliash, and Henry D. I. Abarbanel. Automatic Construction of Predictive Neuron Models through Large Scale Assimilation of Electrophysiological Data. *Scientific Reports*, 6:32749, September 2016.
- [43] Razvan Pascanu, Tomas Mikolov, and Yoshua Bengio. On the difficulty of training recurrent neural networks. In *Proceedings of the 30th International Conference on Machine Learning*, volume 28 of *ICML’13*, pages 1310–1318, Atlanta, GA, USA, June 2013.
- [44] Luka Ribar and Rodolphe Sepulchre. Neuromodulation of Neuromorphic Circuits. *IEEE Transactions on Circuits and Systems I: Regular Papers*, 66(8):3028–3040, August 2019.
- [45] Antônio H. Ribeiro, Koen Tiels, Jack Umberger, Thomas B. Schön, and Luis A. Aguirre. On the smoothness of nonlinear system identification. *Automatica*, 121:109158, November 2020.
- [46] R. Sepulchre, G. Drion, and A. Franci. Control Across Scales by Positive and Negative Feedback. *Annual Review of Control, Robotics, and Autonomous Systems*, 2(1):89–113, 2019.
- [47] Rodolphe Sepulchre, Timothy O’Leary, Guillaume Drion, and Alessio Franci. Control by neuromodulation: A tutorial. In *2019 18th European Control Conference (ECC)*, pages 483–497, June 2019.
- [48] A. A. Sharp, M. B. O’Neil, L. F. Abbott, and E. Marder. Dynamic clamp: computer-generated conductances in real neurons. *Journal of Neurophysiology*, 69(3):992–995, March 1993.
- [49] Jean-Jacques E. Slotine. Modular stability tools for distributed computation and control. *International Journal of Adaptive Control and Signal Processing*, 17(6):397–416, August 2003.
- [50] Ethan Sorrell, Michael E. Rule, and Timothy O’Leary. Brain–Machine Interfaces: Closed-Loop Control in an Adaptive System. *Annual Review of Control, Robotics, and Autonomous Systems*, 4(1):167–189, May 2021.
- [51] David Tsai, Daniel Sawyer, Adrian Bradd, Rafael Yuste, and Kenneth L. Shepard. A very large-scale microelectrode array for cellular-resolution electrophysiology. *Nature Communications*, 8(1):1802, November 2017.

- [52] Hiroyasu Tsukamoto, Soon-Jo Chung, and Jean-Jacques Slotine. Learning-based Adaptive Control via Contraction Theory. *arXiv:2103.02987 [cs, eess, math]*, March 2021.
- [53] I. Y. Tyukin, D. V. Prokhorov, and C. van Leeuwen. Adaptation and Parameter Estimation in Systems With Unstable Target Dynamics and Nonlinear Parametrization. *IEEE Transactions on Automatic Control*, 52(9):1543–1559, September 2007.
- [54] Nina Vogt. Large-scale electrophysiology with polymer-based electrodes. *Nature Methods*, 16(2):143, February 2019.
- [55] Wei Wang and Jean-Jacques E. Slotine. On partial contraction analysis for coupled nonlinear oscillators. *Biological Cybernetics*, 92(1):38–53, December 2004.
- [56] Rafael Yuste, Jason N. MacLean, Jeffrey Smith, and Anders Lansner. The cortex as a central pattern generator. *Nature Reviews Neuroscience*, 6(6):477–483, June 2005.
- [57] Fuzhen Zhang, editor. *The Schur Complement and Its Applications*. Numerical Methods and Algorithms. Springer, Boston, MA, 2005.
- [58] Qinghua Zhang. Adaptive observer for multiple-input-multiple-output (MIMO) linear time-varying systems. *IEEE Transactions on Automatic Control*, 47(3):525–529, March 2002.
- [59] Qinghua Zhang and A. Clavel. Adaptive observer with exponential forgetting factor for linear time varying systems. In *40th IEEE Conference on Decision and Control*, pages 3886–3891, Orlando, FL, USA, December 2001.



Thiago B. Burghi is a post-doctoral researcher in the Control Group of the Department of Engineering at the University of Cambridge. He received the Diplôme d'Ingénieur from ENSTA ParisTech, France, in 2012, and the B.Sc and M.Sc in Control Engineering and Mechanical Engineering, respectively, from the University of Campinas, Brazil, in 2015. He also holds a M.Sc in Robotics from the Pierre and Marie Curie University (Paris VI), France. Thiago was awarded the Capes-Cambridge Trust Scholarship to study

at the University of Cambridge, UK, where he completed his Ph.D in 2020. His research interests lie at the interface between nonlinear control theory, system identification, and biophysical neuronal systems.



Rodolphe Sepulchre (M96,SM08,F10) received the engineering degree and the Ph.D. degree from the Université Catholique de Louvain in 1990 and in 1994, respectively. He is Professor of Engineering at the University of Cambridge since 2013. His research interests are in nonlinear control and optimization, and more recently neuromorphic control. He co-authored the monographs “Constructive Nonlinear Control” (Springer-Verlag, 1997) and “Optimization on Matrix Manifolds” (Princeton

University Press, 2008). He is Editor-in-Chief of IEEE Control Systems. He is a recipient of the IEEE CSS Antonio Ruberti Young Researcher Prize (2008) and of the IEEE CSS George S. Axelby Outstanding Paper Award (2020). He is a fellow of IEEE, IFAC, and SIAM. He has been IEEE CSS distinguished lecturer between 2010 and 2015. In 2013, he was elected at the Royal Academy of Belgium.